

(Draft : April 4, 2018)

Technische Universität Berlin

Institut für Softwaretechnik und Theoretische Informatik
Maschinelles Lernen / Intelligente Datenanalyse

Fakultät IV – Elektrotechnik und Informatik
Franklinstrasse 28-29
10587 Berlin
<http://www.ml.tu-berlin.de>



Master Thesis

Designing Recurrent Neural Networks for Explainability

Pattarawat Chormai

Matriculation Number: 387441
31.03.2018

Supervisor
Prof. Dr. Klaus-Robert Müller

Advisor
Dr. Grégoire Montavon

Acknowledgement

First of all, I would like to thank Prof. Dr. Klaus-Robert Müller and Dr. Grégoire Montavon for this research opportunity and invaluable guidance throughout the course of conducting the thesis as well as facilitating me at TU Berlin, Machine Learning group with a great research environment. I would also like to thank Prof. Dr. Klaus Obermayer and staffs of Neural Information Processing group for organizing Machine Intelligence I & II and Neural Information Project. These courses provide me necessary knowledge to conduct the thesis.

Secondly, I would like to thank my family for always providing me financial and mental support.

Thanks EIT colleagues and . In particular, Someone for proofreading..

I would like to thank EIT Master School as well as TU/e and TUB staffs that involve in this study program. Your support and advice are always helpful.

Lastly, I would like to acknowledge Amazon AWS for generous educational credits and William Vanmoerkerke for lending me a powerful laptop to use in my study. None of experiments would have been possible without these computational support.

Hereby I declare that I wrote this thesis myself with the help of no more than the mentioned literature and auxiliary means.

Berlin, 15.04.2018

.....
Pattarawat Chormai

Abstract

Standard (non-LSTM) recurrent neural networks have been challenging to train, but special optimization techniques such as heavy momentum makes this possible. However, the potentially strong entangling of features that results from this difficult optimization problem can cause deep Taylor or LRP-type to perform rather poorly due to their lack of global scope. LSTM networks are an alternative, but their gating function make them hard to explain by deep Taylor LRP in a fully principled manner. Ideally, the RNN should be expressible as a deep ReLU network, but also be reasonably disentangled to let deep Taylor LRP perform reasonably. The goal of this thesis will be to enrich the structure of the RNN with more layers to better isolate the recurrent mechanism from the representational part of the model.

Zusammenfassung

Da die meisten Leuten an der TU deutsch als Muttersprache haben, empfiehlt es sich, das Abstract zusätzlich auch in deutsch zu schreiben. Man kann es auch nur auf deutsch schreiben und anschließend einem Englisch-Muttersprachler zur Übersetzung geben.

Contents

Notation	xiii
List of Figures	xv
List of Tables	xvii
1 Introduction	1
1.1 Motivation	1
1.2 Objective & Scope	1
1.3 Dataset	2
1.3.1 MNIST	2
1.3.2 FashionMNIST	3
1.4 Outline	4
2 Related Work	5
3 Background	7
3.1 Neural Networks	7
3.1.1 Loss functions	9
3.1.2 Learning Algorithm : Gradient Descent and Backpropagation . . .	9
3.1.3 Convolutional Neural Networks	12
3.1.4 Recurrent Neural Networks	13
3.2 Explainability of Neural Networks	16
3.2.1 Global and Local Explanation	16
3.2.2 Sensitivity Analysis	17
3.2.3 Guided Backpropagation	18
3.2.4 Layer-wise Relevance Propagation	18
3.2.5 Simple Taylor Decomposition	20
3.2.6 Deep Taylor Decomposition	21
4 Experiments	29
4.1 General Setting	29
4.2 Experiment 1 : Sequence Classification	31
4.2.1 Problem Formulation	31
4.2.2 Result	33
4.2.3 Summary	35

4.3	Experiment 2 : Majority Sample Sequence Classification	36
4.3.1	Problem Formulation	36
4.3.2	Evaluation Methodology	38
4.3.3	Result	39
4.3.4	Summary	42
4.4	Experiment 3 : Improve Relevance Propagation	43
4.4.1	Proposal 1 : Stationary Dropout	43
4.4.2	Proposal 2 : Gating units	44
4.4.3	Proposal 3 : Convolutional layer with literal connections	44
4.4.4	Result	45
4.4.5	Summary	52
5	Conclusion	53
5.1	Challenges	53
5.2	Future work	54
References		55
Appendix		59

Notation

θ	Parameters of a neural network
$x, x^{(\alpha)}$	A vector representing an input sample
σ	An activation function
$\{a_j\}_L$	A vector of activations of neurons in layer L
a_j	Activation of neuron j
b_k	Bias of neuron k
R_j	Relevance score of neuron j
$R_{j \leftarrow k}$	Relevance score distributed from neuron k to neuron j
w_{jk}	Weight between neuron j to neuron k
x_i	Feature i of input sample x

List of Figures

1.1	Samples in MNIST	2
1.2	Samples in FashionMNIST	3
3.1	An illustration of how neurons in human brain cooperate together to sense the pain and react accordingly.	7
3.4	Hierarchical features learned by a CNN.	12
3.5	LeNet-5 architecture for a digits recognition task.	12
3.6	Unfolded RNN Structure	13
3.7	LSTM Structure	15
3.8	A classifier classifies “husky” as “wolf” because of the snow background. .	16
3.9	Comparison between global and local explanation	17
3.10	An illustration of relevance propagation in LRP.	19
3.11	Function’s view of R_k and root point candidates	23
3.12	Function’s view of R_k and the root point from z^+ -rule	24
3.13	Function’s view of R_k and the root point from z^β -rule with $-1 < a_j < 1$	25
3.14	Relevance heatmaps from LeNet-5 architecture explained by different explanation methods.	26
4.1	ReLU and Softplus function	29
4.2	RNN Sequence classifier and decision explanation	31
4.3	Shallow and Deep cell architecture with number of neurons at each layer depicted.	32
4.4	Relevance heatmaps from different explanation techniques applied to Shallow and Deep architecture trained on MNIST with different sequence lengths.	34
4.5	Relevance heatmaps from different explanation techniques applied to Shallow and Deep architecture trained on FashionMNIST with different sequence lengths.	35
4.6	Relevance heatmaps of MNIST <i>Class 1</i> and FashionMNIST <i>Class Trouser</i> samples from Shallow-7 and Deep-7 explained by DTD and LRP- $\alpha_{1.5}\beta_{0.5}$. .	36
4.7	Distribution of pixel intensity, relevance quantities from Shallow-7 and Deep-7 propagated by DTD and LRP- $\alpha_{1.5}\beta_{0.5}$ and averaged over MNIST <i>Class 1</i> and FashionMNIST <i>Class Trouser</i> test population.	36
4.8	Majority Sample Sequence Classification(MAJ) problem.	37
4.9	DeepV2 and ConvDeep cell architecture	38

4.10	Comparison between percentage of correctly distributed relevance and cosine similarity.	39
4.11	Relevance heatmaps from different explanation techniques applied to Shallow, Deep, DeepV2 and ConvDeep architecture trained on MNIST-MAJ and FashionMNIST-MAJ with sequence length $T = 12$	41
4.12	Average cosine similarity from different explanation techniques and Shallow, Deep, DeepV2 and ConvDeep architecture.	42
4.13	LSTM with different dropout approaches.	43
4.14	R-LSTM Structure	44
4.15	ConvDeep with literal connections	45
4.16	Relevance heatmaps produced by different explanation techniques on Deep and R-LSTM architecture trained on MNIST-MAJ and FashionMNIST-MAJ with sequence length $T = 12$ and different dropout configurations. .	47
4.17	Average cosine similarity from different explanation techniques and Deep and R-LSTM architecture.	48
4.18	Relevance heatmaps produced by different explanation techniques on variants of ConvDeep and R-LSTM architecture trained on MNIST-MAJ and FashionMNIST-MAJ with sequence length $T = 12$	50
4.19	Positive relevance heatmaps produced by LRP- $\alpha_{1.5}\beta_{0.5}$ technique on R-LSTM and ConvR-LSTM architecture trained on MNIST-MAJ and FashionMNIST-MAJ with sequence length $T = 12$	51
4.20	Average cosine similarity from different explanation techniques and variants of ConvDeep and R-LSTM architecture.	51

List of Tables

3.1	Relevance propagation rules of deep Taylor decomposition.	26
4.1	Summary of hyperparameter.	30
4.2	Minimum classification accuracy for models to be considered.	30
4.3	Dimensions of \boldsymbol{x}_t and number of trainable variables in each cell architecture on sequence length $T = \{1, 4, 7\}$	32
4.4	Accuracy of models trained for sequence classification problem with different sequence lengths and dataset.	33
4.5	Number of trainable variables and model accuracy from architectures trained on MNIST-MAJ and FashionMNIST-MAJ with sequence length $T = 12$	40
4.6	Number of trainable variables and model accuracy of the proposed architectures for MNIST-MAJ and FashionMNIST-MAJ.	46

1 Introduction

1.1 Motivation

In recent years, machine learning has been increasingly involved in almost every aspect of our life, for example recommendation systems on e-commerce sites, cancer diagnosis, or self-driving car. These developments can not be achieved without intelligent algorithms behind. Due to great amount of data and more efficient computational resources, a certain type of machine learning, called neural networks, are directly benefitted and are able to achieve much better performance than traditional machine learning techniques. As a result, many intelligent systems that we use today somehow rely on them.

In short, neural networks are algorithms that are inspired by human. They have units, called neurons, arranged in layers working together to transform input to a desired output. When networks contain many layers, they are referred as deep learning. Connections between neurons define this transformation and will be learned from data. Because the transformation is typically in high dimensional space and built specifically to a certain problem, it is not obvious to us how trained neural networks utilize an input and make a prediction. This lack of understanding raises concerns and questions to the machine learning community and consumers. One major concern is trust to neural network systems, in particular, how we can ensure that the systems will work as we expect. Secondly, without knowing how neural networks process input to the output results in great amount of trials and errors to configure the systems to achieve expected performance.

Several methods have been proposed by researchers in order to better understand or explain how neural networks transforms input to output. Although these work has demonstrated promising results on neural networks, more specifically feed-forward architectures, there is still only a few applications of these methods to recurrent architecture. These recurrent neural networks are considerably important and have been powering almost machine learning systems processing sequential data, such as machine translation and natural language understanding. Therefore, applications of these explanation techniques to recurrent neural networks need to be explored. This results will also enable us to propose adjustments to recurrent architectures such that they are more explainable.

1.2 Objective & Scope

The goal of this thesis is to study how structure of recurrent neural networks affect the quality of explanations produced by various explanation techniques. In particular, the technique that will be experimented are sensitivity analysis(SA), guided backprop(GB),

Layer-Wise Relevance Propagation(LRP) and deep Taylor decomposition(DTD). Our study is based on an artificial classification problem. This problem is specifically constructed such that knowledge of ground truth explanations is available and we can perform qualitative and quantitative measurement accordingly.

The main hypothesis of this thesis is that recurrent neural networks with more layers are more expressible than fewer layers. We extensively conduct experiments on various configurations of recurrent neural network architectures to verify the result. We also propose an adjustment to one of the state-of-the-art recurrent neural network architectures such that it can be explained by the techniques mentioned above.

Lastly, as the primary goal is to study explainability of recurrent neural networks, we do not seek to train models to achieve the state-of-the-art performance. We rather train them to reach a certain level of performance. We assume that models operating in this level would produce comparable explanations.

1.3 Dataset

1.3.1 MNIST

MNIST[LeCun and Cortes, 2010] is one of the most popular dataset that machine learning partitioners use to benchmark machine learning algorithms. The dataset consists of 60,000 training and 10,000 testing samples. Each sample is a grayscale 28x28 image of a digit between from 0 to 9.

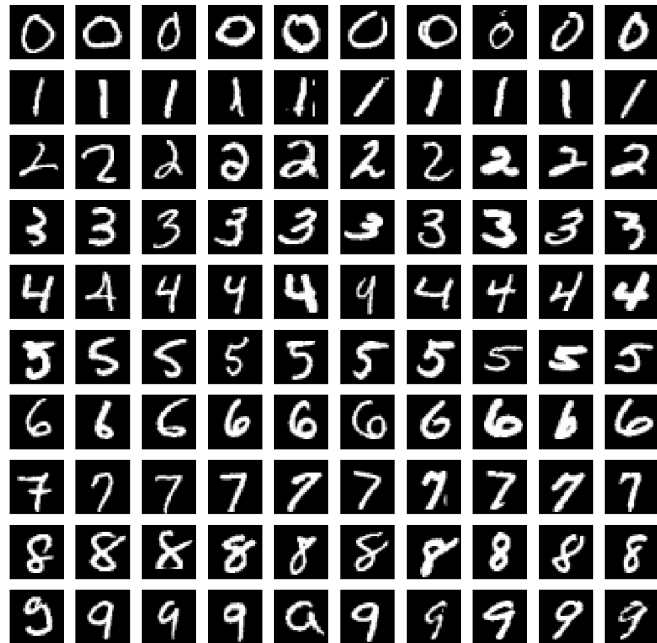


Figure 1.1: Samples in MNIST

State-of-the-art algorithms can classify MNIST with accuracy higher than 0.99, while classical ones, such as SVC or RandomForest, are able to achieve around 0.97[Xiao et al., 2017].

1.3.2 FashionMNIST

Xiao et. al.[Xiao et al., 2017] propose a novel dataset, called FashionMNIST dataset, as a replacement of MNIST dataset for benchmarking machine learning algorithms. According to [Xiao et al., 2017], Fashion-MNIST brings more challenging to the problem and more representative to modern computer vision tasks. It contains images of fashion products from 10 categories. Fashion-MNIST is comparable to MNIST in every aspects, such as the size of training and testing set, image dimension and data format, hence one can easily apply existing algorithms that work with MNIST to Fashion-MNIST without any change.

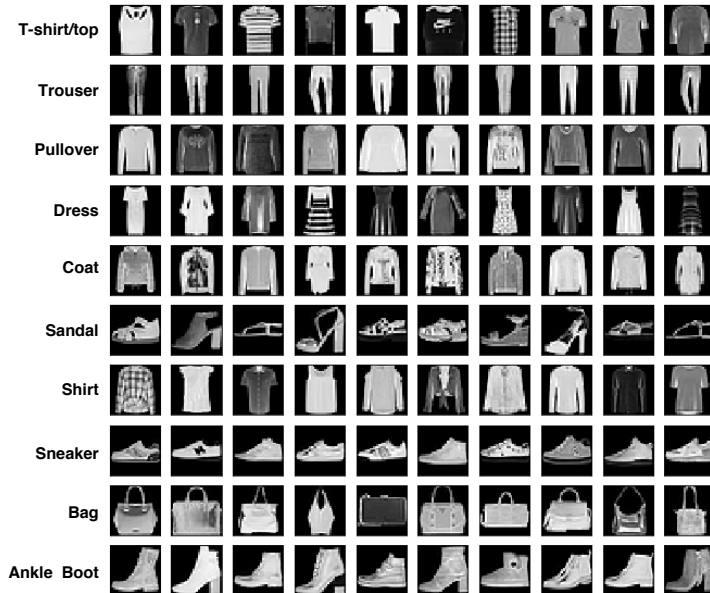


Figure 1.2: Samples in FashionMNIST

[Xiao et al., 2017] also reports benchmarking results of classical machine learning algorithms on Fashion-MNIST. On average, they achieve accuracy between 0.85 to 0.89. According to Fashion-MNIST's page¹, A. Brock reports the state-of-the-art result with 0.97 accuracy using Wide Residual Network(WRN)[Zagoruyko and Komodakis, 2016] and standard data preprocessing and augmentation.

¹<https://github.com/zalandoresearch/fashion-mnist>

1.4 Outline

The thesis is organized as follows :

- **Chapter 2** provides a brief literature survey and related work in the direction towards explaining neural networks.
- **Chapter 3** summaries necessary backgrounds in neural networks and explanation techniques that are discussed in the thesis.
- **Chapter 4** is devoted to experimental results.
- **Chapter 5** concludes the results and discusses challenges as well as future work.

2 Related Work

Neural networks(NN) have been demonstrating their capabilities to solve complex problems in recent years. Recurrent neural networks(RNN) are one of these successful developments. In particular, RNN are designed to process sequential data. Hence, RNN is considerably useful for applications related to text, such as machine translation and natural language processing. In fact, state-of-the-art of these applications today mostly rely on RNN. However, the question of how neural networks, including RNN, derive their predictions is still unclear to us. This causes resistance in the adoption and development of the technology itself.

[Simonyan et al., 2013] proposed a pioneer work in understand the predictions of NN through a method called, *sensitivity analysis*(SA), as well as features that each layer in those networks learn. [Springenberg et al., 2014] suggested a modified version of SA, called *guided backprop*(GB), for ReLU-type neural networks. The result demonstrated that GB produces more meaniful explanations than SA. [Smilkov et al., 2017] also suggested an approach to improve quality of SA explanations. [Bach et al., 2015] proposed an alternative approach, called *Layer-Wise Relevance Propagation*(LRP). The metho utilizes architecture of the neural network itself to create explanations, instead of relying on derivatives as in SA and GB. For ReLU-type networks,[Montavon et al., 2017a] showed that LRP can be equivalent to *deep Taylor decomposition*(DTD). [Sundararajan et al., 2017] proposed *integrated gradients* combining gradient and decomposition technique. [Ribeiro et al., 2016] developed *Local Interpretable Model-Agnostic Explanations*(LIME) that can explain predictions from wider set of models. [Olah et al., 2018] suggested ideas for visualizing explanations from multiple domains.

However, there is still only few work in the direction of explaining predictions from RNN. The only work we have found is from [Arras et al., 2017] where they applied LRP to LSTM[Hochreiter and Schmidhuber, 1997] trained to perform a sentiment analysis task.

3 Background

3.1 Neural Networks

Neural networks(NNs) are a type of machine learning algorithms that try to mimic how human brain works. In particular, NNs have units called neurons connecting together similar to the way neurons in our brain do. These connections allow NNs to build hierarchical representations that are necessary to perform an objective task. Figure 3.1 illustrates a simple reaction task that neurons in our brain perform together to achieve.

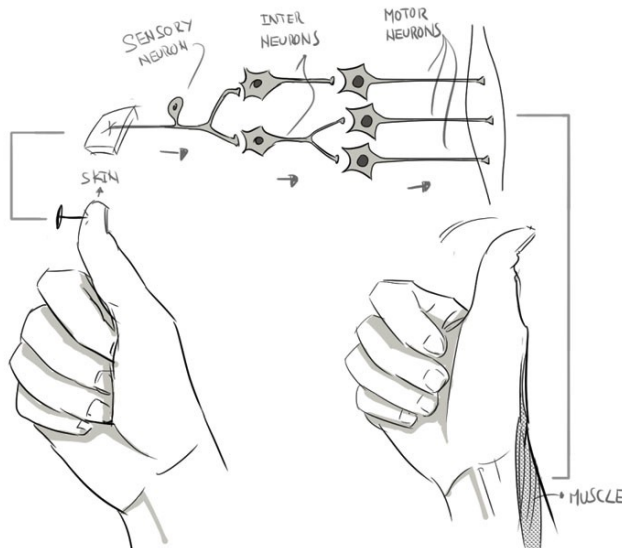


Figure 3.1: An illustration of how neurons in human brain cooperate together to sense the pain and react accordingly.

Source : [Leon, 2017]

Figure 3.2 illustrates a general structure of NNs. The network has input layer, output layer and hidden layers, which are analogous to sensory, motor and inter neurons in Figure 3.1. The figure also shows connections of a neuron to other neurons in previous and later layer. Given an objective task, the goal is to construct connections between these neurons such that the network can transform input into a desired output. These connections are determined by trainable variables, called weights and biases. They are denoted by $w_{i \rightarrow j}$, $w_{j \rightarrow k}$ and b_j respectively in the figure, and will be learned in during *training* process. In this example, the objective task to classify what is the given digit.

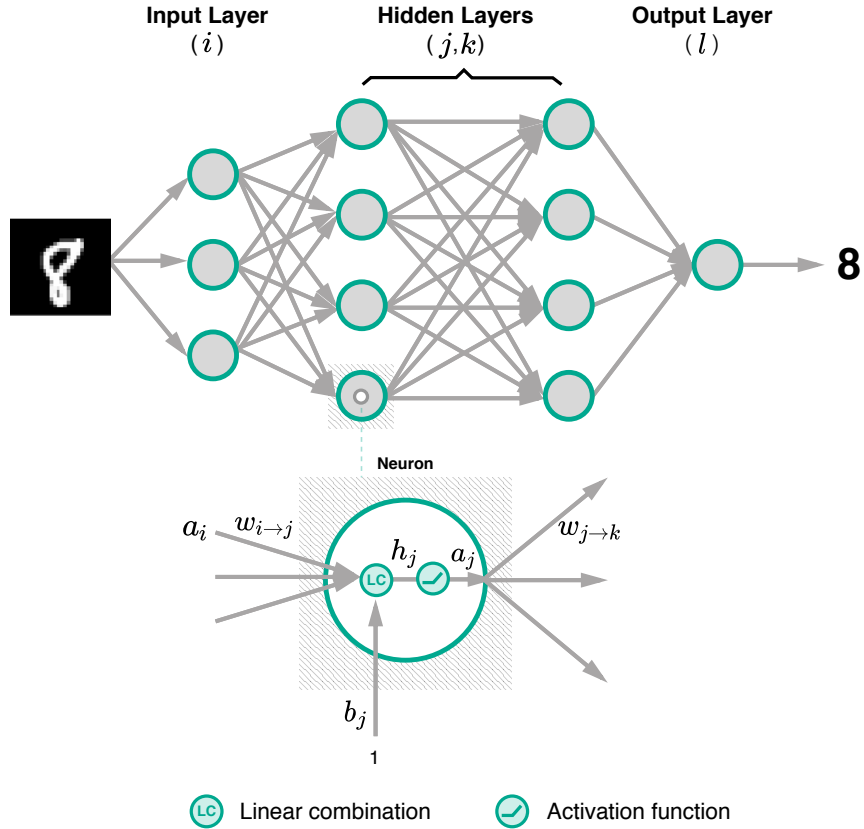


Figure 3.2: A general structure of neural networks and details of a neuron's connectivity and activity.

Consider a given set of p training samples $\mathcal{D} = \{\mathbf{x}^{(\alpha)}, y^{(\alpha)}\}_{\alpha=1}^p$, there are 3 primary components to train a NN, namely

1. **Network architecture** defines the configuration of NN. Some of important settings are number of layers and number of neuron in each layer and type of activation function. These settings determine neurons' activity and how they communicate to each other through connections governed by trainable weights and biases. Typically, the weights and biases are denoted as $\boldsymbol{\theta}$. Mathematically, NN can be viewed as a function f with parameters $\boldsymbol{\theta}$ that nonlinearly transforms an input $\mathbf{x}^{(\alpha)} \in \mathbb{R}^d$ to some output.
2. **Loss function L** is a measurement corresponding to the objective task. It quantifies how far output $f(\mathbf{x}^{(\alpha)})$ from the NN far the true output $y^{(\alpha)}$. If we average the loss over some samples, we call the result as *Cost* and denote it as J .
3. **Learning algorithm** is responsible for optimizing trainable variables in the net-

work such that the overall loss is minimized. Practically, we learn this variables through optimizing the cost of training samples *Empirical Error*. This is a proxy to optimize the cost of the data distribution(*Generalization Error*).

Hence, the goal of this empirical training process can be summarized as follows :

$$\hat{\boldsymbol{\theta}} = \underset{\boldsymbol{\theta}}{\operatorname{argmin}} \underbrace{\frac{1}{p} \sum_{\alpha=1}^p L(f(\mathbf{x}^{(\alpha)}), y^{(\alpha)})}_{J} \quad (3.1)$$

3.1.1 Loss functions

Choosing loss function is depend on the objective that the network is being trained to solve. For classification problems, such as digit classification, whose goal is to categorize \mathbf{x} into a category C from K categories, $f : \mathbf{x} \in \mathbb{R}^d \mapsto C \in \{C_k\}_{k=1}^K$, *Cross-Entropy*(CE) is the loss function for this purpose.

$$L_{\text{CE}} = - \sum_i y_k \log \hat{y}_k,$$

where $y_i \in [0, 1]$ and $\hat{y}_i \in [0, 1]$ are true and predicted probability that \mathbf{x} belongs to C_k respectively. Denote $\mathbf{z} = f(\mathbf{x}) \in \mathbb{R}^K$. \hat{y}_k is computed via *softmax* function :

$$\hat{y}_k = \frac{e^{z_k}}{\sum_{k=1}^K e^{z_k}}$$

For regression problems, $f : \mathbf{x} \in \mathbb{R}^d \mapsto \mathbb{R}$, such as price forecast, *Mean Squared Error*(MSE) is the loss function.

$$L_{\text{MSE}} = (f(\mathbf{x}) - y)^2$$

This is a brief introduction to loss functions widely used in machine learning. More loss functions do exist and are beyond scope of the thesis to cover.

3.1.2 Learning Algorithm : Gradient Descent and Backpropagation

Due to substantial number of trainable variables in a neural network, it is crucial to solve the optimization (3.1) efficiently. The answer to solve this high dimensional problem is to use repeated procedure, called *Gradient Descent*. Figure 3.3 provides an intuition of the method. Consider a function $J(\boldsymbol{\theta})$ on the figure as a toy example of a cost function of a NN with a parameter $\boldsymbol{\theta}$. The figure shows that if we gradually adjust $\boldsymbol{\theta}$ in the opposite direction of gradient, $-\frac{dL(\boldsymbol{\theta})}{d\boldsymbol{\theta}}$, with a proper step size λ (*learning rate*), we will eventually reach one of the minimals. This update is summarized in (3.2).

$$\theta_i \leftarrow \theta_i - \lambda \frac{\partial J}{\partial \theta_i}, \forall \theta_i \in \boldsymbol{\theta} \quad (3.2)$$

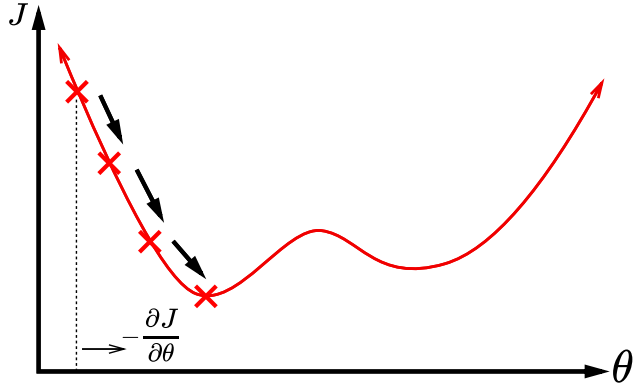


Figure 3.3: An illustration of Gradient Descent

Let's consider again the NN shown in Figure 3.2. Assume that the network uses an activation function σ and has $\theta = \{\forall i, j, k, l : w_{i \rightarrow j}^{(1)}, w_{j \rightarrow k}^{(2)}, w_{k \rightarrow l}^{(3)}\}$ with biases omitted. For a sample $(\mathbf{x}^{(\alpha)}, y^{(\alpha)})$, $f(\mathbf{x}^{(\alpha)})$ is calculated as follows

$$\begin{aligned}
 h_j^{(1)} &= \sum_i w_{i \rightarrow j}^{(1)} x_i^{(\alpha)} & a_j^{(1)} &= \sigma(h_j^{(1)}) \\
 h_k^{(2)} &= \sum_j w_{j \rightarrow k}^{(2)} a_j^{(1)} & a_k^{(2)} &= \sigma(h_k^{(2)}) \\
 h_l^{(3)} &= \sum_k w_{k \rightarrow l}^{(3)} a_k^{(2)} & a_l^{(3)} &= \sigma(h_l^{(3)}) \\
 f(\mathbf{x}) &= [a_1^{(3)}, \dots, a_L^{(3)}]^T & J &= \frac{1}{p} \sum_{\alpha=1}^p L(f(\mathbf{x}^{(\alpha)}), y^{(\alpha)})
 \end{aligned}$$

The gradients can be then computed by recursively applying chain rule from the last

to the first layer, hence the name *Backpropagation*.

$$\frac{\partial l(f(\mathbf{x}^{(\alpha)}), y^{(\alpha)})}{\partial w_{k \rightarrow l}^{(3)}} = \frac{\partial l(f(\mathbf{x}^{(\alpha)}), y^{(\alpha)})}{\partial a_l^{(3)}} \frac{\partial a_l^{(3)}}{\partial w_{k \rightarrow l}^{(3)}} \quad (3.3)$$

$$= \underbrace{\frac{\partial l(f(\mathbf{x}^{(\alpha)}), y^{(\alpha)})}{\partial a_l^{(3)}}}_{\delta_l^{(3)}} \sigma'(h_l^{(3)}) a_k^{(2)} \quad (3.4)$$

$$\frac{\partial l(f(\mathbf{x}^{(\alpha)}), y^{(\alpha)})}{\partial w_{j \rightarrow k}^{(2)}} = \sum_{l'=1}^L \frac{\partial l(f(\mathbf{x}^{(\alpha)}), y^{(\alpha)})}{\partial a_{l'}^{(3)}} \frac{\partial a_{l'}^{(3)}}{\partial w_{j \rightarrow k}^{(2)}} \quad (3.5)$$

$$= \sum_{l'=1}^L \frac{\partial l(f(\mathbf{x}^{(\alpha)}), y^{(\alpha)})}{\partial a_{l'}^{(3)}} \sigma'(h_{l'}^{(3)}) \frac{\partial h_{l'}^{(3)}}{\partial w_{j \rightarrow k}^{(2)}} \quad (3.6)$$

$$= \sum_{l'=1}^L \delta_{l'}^{(3)} w_{k \rightarrow l'}^{(3)} \frac{\partial a_k^{(2)}}{\partial w_{j \rightarrow k}^{(2)}} \quad (3.7)$$

$$= a_j^{(1)} \underbrace{\sigma'(h_k^{(2)}) \sum_{l'=1}^L \delta_{l'}^{(3)} w_{k \rightarrow l'}^{(3)}}_{\delta_k^{(2)}} \quad (3.8)$$

$$\frac{\partial l(f(\mathbf{x}^{(\alpha)}), y^{(\alpha)})}{\partial w_{i \rightarrow j}^{(1)}} = x_i \sigma'(h_j^{(1)}) \sum_{k'=1}^K \delta_{k'}^{(2)} w_{j \rightarrow k'}^{(2)} \quad (3.9)$$

As shown in the derivations above, *Backpropagation* allows us to efficiently compute the gradients by reusing calculated gradients from the later layer, for example $\delta_l^{(3)}, \delta_k^{(2)}$. Moreover, $\delta_l^{(3)}, \delta_k^{(2)}$ can also interpreted as error propagated to responsible neurons.

In practice, because the training set usually contains several thousand samples, the gradient update in (3.2) would require significant amount of computation to update just one step, not to mention that it could also result in small gradient update step leading to slow convergence to desire objective performance. Therefore, the training data D is usually divided into batches \tilde{D}_i with equal size and perform the gradient update for every \tilde{D}_i . For example, the size of \tilde{D}_i is usually chosen between 32 and 512 samples. This refers to *Mini-Batch Gradient Descent*.

Lastly, because noise in training data and potentially highly non-smooth of the cost function, learning rate λ has great influential on the training process. More precisely, it should not be too small or too large. This requires some effort and experience in order to get the right value. Some work have proposed alternative update rules aiming to make the training process more stable. For example, Adaptive Moment Estimation(Adam)[Kingma and Ba, 2014] uses adaptive learning rate and incorporates accumulated direction and speed of the previous gradients(*momentum*) into the update, hence more consistent gradient and fast convergence. Other similar proposals are RMSProp

[Tieleman and Hinton, 2012] and Adadelta [Zeiler, 2012].

3.1.3 Convolutional Neural Networks

Convolutional Neural Networks(CNNs) refer to neural networks that employ convolutional operators to process information in early layers instead of fully-connected layers(weighted sum). Typically, a convolutional operator is followed by a pooling operator. Using this convolutional and pooling operators allows the neural network to extract hierarchical features that are spatially invariant [Zeiler and Fergus, 2013], hence leading to higher predictive capability comparing to traditional fully-connected layers with fewer number of parameters.

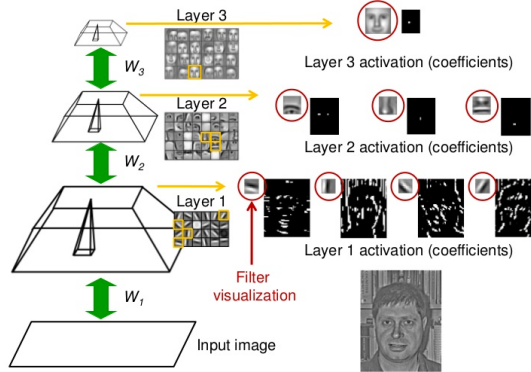


Figure 3.4: Hierarchical features learned by a CNN.

Source : [Lee et al., 2009]

Figure 3.4 illustrates hierarchical structures that neurons in each layer of a CNN learn to detect. More precisely, this example shows that neurons in the first learn to detect low level features, such as edges, and neurons in middle layer then use knowledge to detect higher level features, for example nose, mouth or eyes, and so on.

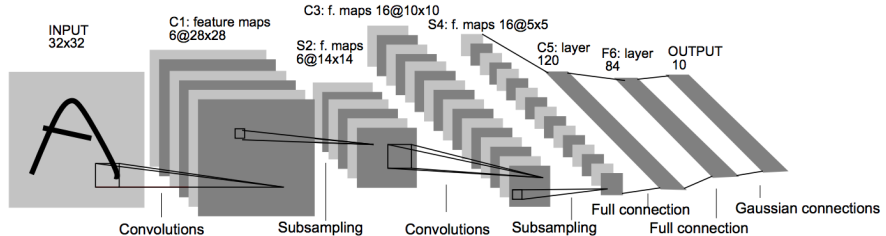


Figure 3.5: LeNet-5 architecture for a digits recognition task.

Source : [LeCun et al., 2001]

Since [LeCun et al., 2001] proposed LeNet-5, shown in Figure 3.5, and successfully

applied it to handwritten recognition problems, CNNs have become the first choice of architectures in many domains. Particularly, in computer vision, CNNs are the core component of state-of-the-art results in various contests. Such successful results are : AlexNet[Krizhevsky et al., 2012] that archive the remarkable results on ImageNet Large-Scale Visual Recognition Challenge 2012(ILSVRC 2012) followed by the achievement of VGG[Simonyan and Zisserman, 2014] and GoogleLenet [Szegedy et al., 2014] architecture in ILSVRC 2014 and ResNet[He et al., 2015] that won ILSVRC 2015.

3.1.4 Recurrent Neural Networks

Recurrent Neural Networks(RNNs) are neural networks whose computed outputs are repeatedly incorporated into its next computation. Figure 3.6 illustrates this idea of recurrent computation by unfolding RNN into steps. Let's consider \mathbf{x} a sequence of x_1, \dots, x_T . At step t , RNN takes r_{t-1} and x_t to compute r_t and \hat{y}_t . This recurrent connections can be interpreted as accumulating information from the past, hence RNNs are well capable of processing sequential data, possibly coming with different and not limited in length . Natural Language Processing(NLP) and Machine Translation(MT) are some of the fields that RNNs are widely applied to.

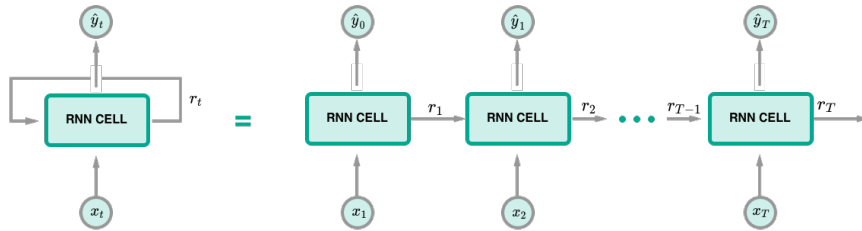


Figure 3.6: Unfolded RNN Structure
Inspired by a figure in [Olah, 2015]

Backpropagation Through Time

As the number of computation steps in RNNs is depend on the length of samples, which can be different in principle, one needs to organize data in such a way that samples in the same batch have the same steps of computations before training a RNN. As a result, training RNNs can be viewed as training a feedforward neural network with a certain depth of layers, where we can then apply backpropagation. The difference from regular feedforward setting is that variables are shared across layers.

Consider again the RNN in Figure 3.6 with $\mathbf{x} = \{x_1, \dots, x_T\}$ and $r_0 = 0$. Assume that only \hat{y}_T determines the value of the loss function and the computations are defined

as follows

$$h_1 = w_{rx}x_1 + w_{rr}r_0 \quad r_1 = \sigma(h_1) \quad (3.10)$$

$$h_2 = w_{rx}x_2 + w_{rr}r_1 \quad r_2 = \sigma(h_2) \quad (3.11)$$

$$\vdots \quad \vdots \quad (3.12)$$

$$h_{T-1} = w_{rx}x_{T-1} + w_{rr}r_{T-2} \quad r_{T-1} = \sigma(h_{T-1}) \quad (3.13)$$

$$\hat{y} = \sigma(w_{yx}x_T + w_{yr}r_{T-1}) \quad (3.14)$$

The gradients can be computed by

$$\frac{\partial l}{\partial w_{yx}} = \sigma'(w_{yx}x_T + w_{yr}r_{T-1})x_T \quad (3.15)$$

$$\frac{\partial l}{\partial w_{yr}} = \sigma'(w_{yx}x_T + w_{yr}r_{T-1})r_{T-1} \quad (3.16)$$

$$\frac{\partial l}{\partial w_{rx}} = w_{yr}\sigma'(w_{yx}x_T + w_{yr}r_{T-1})\frac{\partial r_{T-1}}{\partial w_{rx}} \quad (3.17)$$

$$= w_{yr}\sigma'(w_{yx}x_T + w_{yr}r_{T-1})\left[\sigma'(h_{T-1})\left(x_{T-1} + w_{rr}\frac{\partial r_{T-2}}{\partial w_{rx}}\right)\right] \quad (3.18)$$

$$\frac{\partial l}{\partial w_{rr}} = w_{yr}\sigma'(w_{yx}x_T + w_{yr}r_{T-1})\frac{\partial r_{T-1}}{\partial w_{rr}} \quad (3.19)$$

$$= w_{yr}\sigma'(w_{yx}x_T + w_{yr}r_{T-1})\left[\sigma'(h_{T-1})\left(\frac{\partial r_{T-2}}{\partial w_{rr}}\right)\right] \quad (3.20)$$

$$(3.21)$$

However, as we unfold the computations, we can see that there are 2 problems that might happen to the gradients of the shared parameters w_{rx} and w_{rr} , namely

- Exploding Gradient : this scenario happens if the gradient is derived from shared weights, for example w_{rr} in (3.18), whose absolute value is greater than one. The recursive multiplication will result in a large value of the gradient leading to unreliable training. [Pascanu et al., 2012] have proposed Gradient Clipping to alleviate the problem.
- Varnishing Gradient : in contrast, when the values are smaller than one, the gradient will be very small causing slow learning. More precisely, RNNs would require enormous of time to learn long term dependencies. The next section discusses techniques to mitigate this problem.

Long Short-Term Memory and Gated RNNs

Varnishing Gradient is a major problem that causes RNNs to learn long term memories with slow progress. This is due to the computation of recurrent connections are constructed. In particular, as in (3.10), standard RNNs compute those connections with

weighted sum at every step t leading to recursive multiplication terms in the gradient's computation.

Alternatively, [Hochreiter and Schmidhuber, 1997] have proposed *Long Short-Term Memory*(LSTM) network that employs a gating mechanism and additive updates in the calculation of the recurrent connections. This mechanism decreases number of damping factors involved in the gradients' computation, hence it allows the network to learn long memories better.

As shown in Figure 3.7, LSTM utilizes 3 gates, namely input i_g , forget f_g and o_g output gate, to control the information flow through the LSTM cell. More precisely, i_g and f_g decides how to accumulate information from the previous cell state C_{t-1} , and an input cell state computed from previous output h_{t-1} and current input x_t , into the new cell state C_t . On the other hand, o_g determines to control leakage of information from C_t to outside h_t . Formally,

$$i_g = \sigma(w_{ix}x_t + w_{ih}h_{t-1}) \quad (3.22)$$

$$o_g = \sigma(w_{ox}x_t + w_{oh}h_{t-1}) \quad (3.23)$$

$$C_t = f_g \otimes C_{t-1} + i_g \otimes \tilde{C}_t \quad (3.24)$$

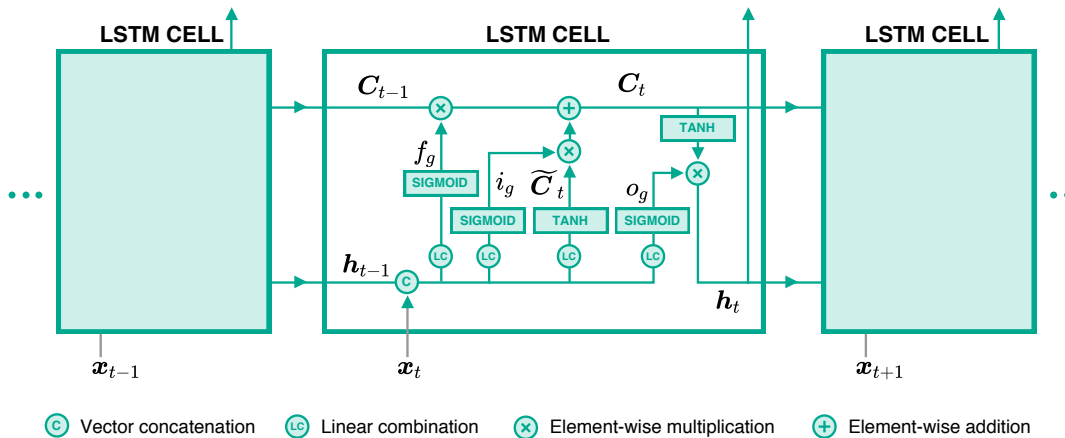


Figure 3.7: LSTM Structure

Since the work was published, LSTM has successfully contributed to many state-of-the-art results in Machine Translation(MT) and Natural Language Processing(NLP)[Melis et al., 2018]. [Greff et al., 2017] have shown that the forget and output gate are the crucial parts of the network. [Cho et al., 2014] have proposed *Gated Recurrent Unit*(GRU) that employs only 2 gates, however [Jozefowicz et al., 2015] have conducted several benchmarking tasks and found no significant difference in performance between LSTM and GRU.

3.2 Explainability of Neural Networks

Neural networks have become one of major machine learning algorithms used in many applications, for example computer vision and medicine. Despite those achievements, they are still considered as a blackbox process that is difficult to interpret its results or find evidences that the networks use to make such accurate decisions for further analyses.

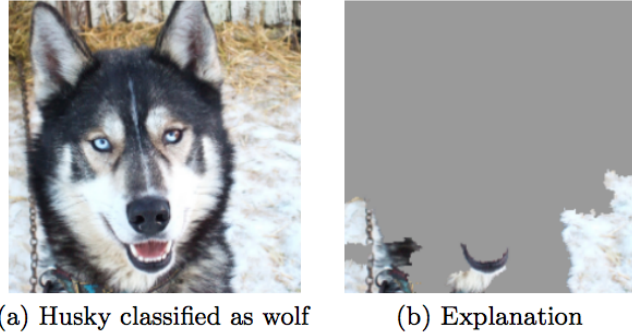


Figure 3.8: A classifier classifies “husky” as “wolf” because of the snow background.
Source : [Ribeiro et al., 2016]

Moreover, it is always important to verify whether trained neural networks properly utilize data or what information it uses to make decisions. Literatures refer this functional inspection as “Explainability” or “Interpretability”. [Bach et al., 2016, Ribeiro et al., 2016] demonstrated that there are cases that some neural networks exploit artifacts in the data to make decisions. Figure 3.8 is such an example. This discoveries emphasize the importance of having explainable neural networks, not to mention the fact that nowadays neural networks have involved in several aspects that human’s life is involved, such as medicine or self-driving car. Therefore, having more explainable models is necessary.

3.2.1 Global and Local Explanation

Formally, interpreting neural networks can analyze in 2 approaches, namely *global* and *local* explanation. Consider an image classification problem of \mathcal{C} classes, global explanation aims to find an image \mathbf{x}^* that is the most representative to a class $c_i \in \mathcal{C}$. Activation Maximization[Erhan et al., 2010] is one of the method in this category.

$$\mathbf{x}^* = \underset{\mathbf{x}}{\operatorname{argmax}} \mathbb{P}(c|\mathbf{x}, \theta) \quad (3.25)$$

On the other hand, local explanation focuses on finding relevant information in \mathbf{x} that can explain why the neural network predicts that \mathbf{x} belongs to a certain class $c_i \in \mathcal{C}$. More precisely, local explanation seeks to assign each pixel $x_i \in \mathbf{x}$ with a score that quantitatively explains how the pixel influences the neural network to make a decision.

The score is formally referred as *relevance score* and denoted with $R_i(\mathbf{x})$ or R_i if it is clear from the context. As a result, combining $R_i(\mathbf{x})$ together will produce a *relevance heatmap* or *explanation heatmap*.

As illustrated in Figure 3.9, the difference between global and local explanation can be analogously described by formulating questions as follows

- Global explanation : “Hoes does a usual lamp look like?”
- Local explanation : “which area in the image make it look like a lamp?”

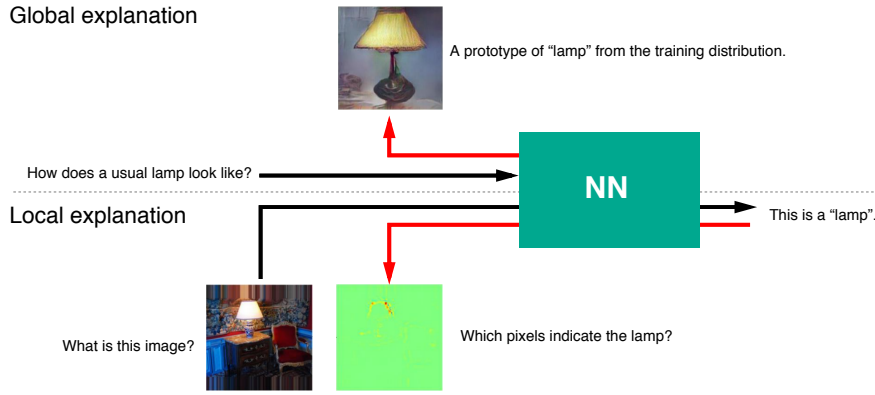


Figure 3.9: Comparison between global and local explanation

The analogy is borrowed from Prof. Müller's lecture slide.

The images were taken from [Nguyen et al., 2016, Bach et al., 2015].

In the following, we are going to discuss approaches in local explanation in details and leave content of global explanation aside due to scope of the thesis. In particular, we are going to introduce these local explanation methods, namely *sensitivity analysis*, *guided backprop*, *simple Taylor decomposition*, *Layer-wise Relevance Propagation* and *deep Taylor decomposition*.

3.2.2 Sensitivity Analysis

Sensitivity analysis(SA)[Simonyan et al., 2013] is a local explanation that derives relevance score $R_i(\mathbf{x})$ through the partial derivative of $f(\mathbf{x})$ respect to x_i . In particular, it is formulated as follows

$$R_i(\mathbf{x}) = \left(\frac{\partial f(\mathbf{x})}{\partial x_i} \right)^2 \quad (3.26)$$

which can then be interpreted as

$$\sum_i R_i(\mathbf{x}) = \|\nabla f(\mathbf{x})\|^2 \quad (3.27)$$

The derivation of $\sum_i R_i(\mathbf{x})$ above implies that SA seeks to explain $R_i(\mathbf{x})$ from the aspect of variation magnitudes of $f(\mathbf{x})$, which might not reflect the actual influence of the pixels to the decision.

However, this technique can be easily implemented in modern deep learning frameworks, such as TensorFlow[Abadi et al., 2016], via automatic differentiation. Hence, one might consider it to as a first tool towards explainability of neural networks.

3.2.3 Guided Backpropagation

Guided backpropagation(GB) is a extended version of sensitivity analysis where gradients are propagated throughout the network in a controlled manner. It is specifically designed for neural networks that use piecewise linear activations, such as ReLU. Formally, [Springenberg et al., 2014] proposed an alternative definition of ReLU function as

$$\sigma(a_j) = a_j \mathbb{1}[a_j > 0], \quad (3.28)$$

where $\mathbb{1}[\cdot]$ is an indicator function, and defined a new derivative of a ReLU neuron j as:

$$\frac{\partial_* f(\mathbf{x})}{\partial a_j} = \mathbb{1}\left[a_j > 0\right] \mathbb{1}\left[\frac{\partial f(\mathbf{x})}{\partial a_j} > 0\right] \frac{\partial f(\mathbf{x})}{\partial a_j} \quad (3.29)$$

From the derivation above, $\mathbb{1}[\cdot]$ controls whether original gradients are propagated back, in particular, the gradients will be propagated to the previous layer only if neuron j is active and the gradient from the next layer is positive. Similar to SA, the relevance score for each pixel is computed as

$$R_i(\mathbf{x}) = \left(\frac{\partial_* f(\mathbf{x})}{\partial x_i} \right)^2 \quad (3.30)$$

3.2.4 Layer-wise Relevance Propagation

The methods mentioned so far derive $R_i(\mathbf{x})$ directly from $f(\mathbf{x})$ and do not use important knowledge about the network itself, such as architecture or activation values. Alternatively, Bach et al.[Binder et al., 0906] propose Layer-wise Relevance Propagation(LRP) framework that leverages this known information to distribute relevance scores to x_i . In particular, LRP propagates relevance scores backward from layer to layer, similar to the back-propagation algorithm of gradient descent.

Consider the neural network illustrated in Figure 3.10. R_j and R_k are relevance score of neurons j, k in successive layers. LRP provides a general form of relevance propagation as

$$R_j = \sum_k \delta_{j \leftarrow k} R_k, \quad (3.31)$$

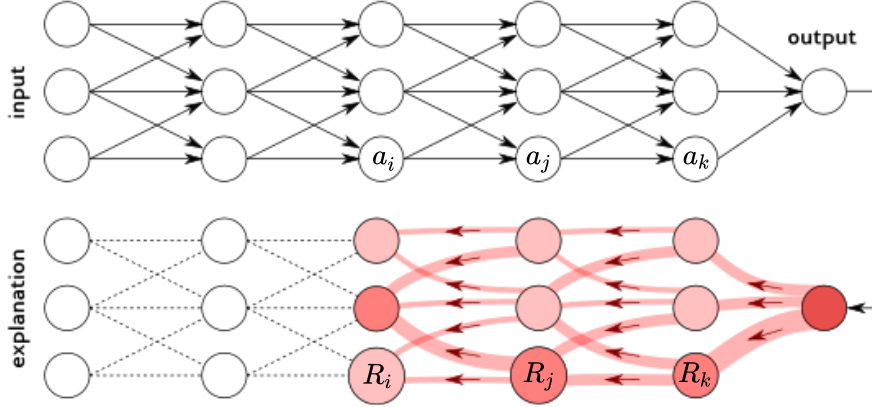


Figure 3.10: An illustration of relevance propagation in LRP.
Source : <http://heatmapping.org>

where $\delta_{j \leftarrow k}$ defines a proportion that R_k contributes to R_j . Consider further that activity a_k of neuron k is computed by

$$a_k = \sigma \left(\sum_j w_{jk} a_j + b_k \right), \quad (3.32)$$

where σ is a activation function, w_{jk}, b_k are the corresponding weight and bias between neuron j and k . For monotonic increasing σ , $\delta_{j \leftarrow k}$ can be calculated as follows

$$\delta_{j \leftarrow k} = \alpha \frac{a_j w_{jk}^+}{\sum_j a_j w_{jk}^+} - \beta \frac{a_j w_{jk}^-}{\sum_j a_j w_{jk}^-}, \quad (3.33)$$

where w_{jk}^+ , w_{jk}^- are $\max(0, w_{jk})$, $\min(0, w_{jk})$, and α, β are parameters with $\alpha - \beta = 1$ restriction. Combining (3.31) and (3.33) results in LRP- $\alpha\beta$ rule,

$$R_j = \sum_k \left(\alpha \frac{a_j w_{jk}^+}{\sum_j a_j w_{jk}^+} - \beta \frac{a_j w_{jk}^-}{\sum_j a_j w_{jk}^-} \right) R_k \quad (3.34)$$

Algorithm 1 summaries how LRP works.

Algorithm 1: LRP Algorithm

```

 $f(\mathbf{x}), \{\{a\}_{l_1}, \{a\}_{l_2}, \dots, \{a\}_{l_n}\} = \text{forward\_pass}(\mathbf{x}, \boldsymbol{\theta});$ 
 $R_k = f(\mathbf{x});$ 
for  $\text{layer} \in \text{reverse}(\{l_1, l_2, \dots, l_n\})$  do
     $\text{prev\_layer} \leftarrow \text{layer} - 1;$ 
    for  $j \in \text{neurons}(\text{prev\_layer}), k \in \text{neurons}(\text{layer})$  do
         $| R_j \leftarrow \text{LRP-}\alpha\beta(R_k, \{a\}_j, \{w\}_{j,k})$ 
    end
end

```

Alternatively, if we slightly rearrange the rule to

$$R_j = \sum_k \left(\frac{a_j w_{jk}^+}{\sum_j a_j w_{jk}^+} \hat{R}_k + \frac{a_j w_{jk}^-}{\sum_j a_j w_{jk}^-} \check{R}_k \right),$$

where $\hat{R}_k = \alpha R_k$ and $\check{R}_k = -\beta R_k$. We can then intuitively interpret this propagation as

“Relevance \hat{R}_k ” should be redistributed to the lower-layer neurons $\{a_j\}_j$ in proportion to their excitatory effect on a_k . “Counter-relevance” \check{R}_k should be redistributed to the lower-layer neurons $\{a_j\}_j$ in proportion to their inhibitory effect on a_k - Section 5.1 [Montavon et al., 2017b]

Moreover, LRP has *Conservation Property* in which relevance quantities are conserved during distributing $f(\mathbf{x})$ back to \mathbf{x} . Formally, it is

$$\sum_i R_i = \dots = \sum_j R_j = \sum_k R_k = \dots = f(\mathbf{x}) \quad (3.35)$$

Nonetheless, choices of α, β is still a question for LRP. In particular, [Montavon et al., 2017b, Binder et al., 0906] demonstrated that the influence of the values to explanation heatmaps are depend on network architecture. For example, [Montavon et al., 2017b] observed that LRP- α_1, β_0 works well for deep architectures, such as GoogleNet[Szegedy et al., 2014], while LRP- α_2, β_1 is better for shallower architectures, such as BVLC CaffeNet[Jia et al., 2014].

3.2.5 Simple Taylor Decomposition

As the name suggested, the method decomposes $f(\mathbf{x})$ using Taylor series around the root point $\tilde{\mathbf{x}}$ where the relevance scores $R_i(\mathbf{x})$ are the first order terms of the series.

$$f(\mathbf{x}) = f(\tilde{\mathbf{x}}) + \underbrace{\sum_i \frac{\partial f}{\partial x_i} \Big|_{x_i=\tilde{x}_i} (x_i - \tilde{x}_i)}_{R_i} + \zeta, \quad (3.36)$$

where ζ are the second and higher order terms that are not considered here. The root point $\tilde{\mathbf{x}}$ can be found via the optimization below

$$\min_{\xi \in \mathcal{X}} \|\xi - \mathbf{x}\|^2 \quad \text{such that } f(\xi) = 0, \quad (3.37)$$

where \mathcal{X} represents the input distribution. This optimization is time consuming and ξ might potentially be **TODO : Check property : close to** or diverge from \mathbf{x} leading to non informative R_i . However, for neural networks using piecewise linear activations, such as ReLU, $\tilde{\mathbf{x}}$ can be computed analytically. In particular, with assumptions of

$\sigma(tx) = t\sigma(x)$, $\forall t \geq 0$ and no use of bias, [Montavon et al., 2017b] argued that $\tilde{\mathbf{x}}$ can be found in approximately the same flat region as \mathbf{x} , $\tilde{\mathbf{x}} = \lim_{\epsilon \rightarrow 0} \epsilon \mathbf{x}$, yielding

$$\frac{\partial f(\mathbf{x})}{\partial x_i} \Big|_{\mathbf{x}=\tilde{\mathbf{x}}} = \frac{\partial f(\mathbf{x})}{\partial x_i} \Big|_{\mathbf{x}=\mathbf{x}} \quad (3.38)$$

As a result, (3.36) can be simplified to :

$$f(\mathbf{x}) = \sum_i \frac{\partial f(\mathbf{x})}{\partial x_i} \Big|_{\mathbf{x}=\mathbf{x}} x_i \quad (3.39)$$

$$R_i = \frac{\partial f(\mathbf{x})}{\partial x_i} \Big|_{\mathbf{x}=\mathbf{x}} x_i \quad (3.40)$$

One can also interpret the relationship between sensitivity analysis and simple Taylor decomposition from (3.40). Specifically, x_i has high relevance score if x_i highly activates and its variation positively affects $f(x)$ and vice versa.

3.2.6 Deep Taylor Decomposition

Using Taylor decomposition as a foundation, deep Taylor decomposition(DTD) is a explanation technique that decomposes R_k into Taylor series where R_j from previous layer are the first order terms. [Montavon et al., 2017a] proposed the method to explain decisions of neural networks with piece-wise linear activations. Similar to LRP, DTD repeatedly decomposes relevances at the last layer R_k and propagates the quantities to R_j in the previous layer until the relevance of input pixel $R_i(\mathbf{x})$. In particular, R_k is decomposed as follows :

$$R_k = R_k \Big|_{\tilde{\mathbf{a}}_j} + \sum_j \frac{\partial R_k}{\partial a_j} \Big|_{a_j=\tilde{a}_j} (a_j - \tilde{a}_j) + \zeta_k \quad (3.41)$$

Assume further that there exists a root point $\tilde{\mathbf{a}}_j$ such that $R_k = 0$, and the second and higher terms $\zeta_k = 0$. Then, (3.41) can be reduced to

$$R_k = \sum_j \underbrace{\frac{\partial R_k}{\partial a_j} \Big|_{a_j=\tilde{a}_j} (a_j - \tilde{a}_j)}_{R_{j \leftarrow k}} \quad (3.42)$$

As the relevance propagated back, R_j is $\sum_k R_{j \leftarrow k}$ from neuron k in the next layer

that neuron j contributes to. Hence, DTD has *Conservation Property*,

$$R_j = \sum_k R_{j \leftarrow k} \quad (3.43)$$

$$\sum_j R_j = \sum_j \sum_k R_{j \leftarrow k} \quad (3.44)$$

$$\sum_j R_j = \sum_k \sum_j R_{j \leftarrow k} \quad (3.45)$$

$$\sum_j R_j = \sum_k R_k \quad (3.46)$$

$$\sum_i R_i = \dots = \sum_j R_j = \sum_k R_k = \dots = f(\mathbf{x}) \quad (3.47)$$

Finding the root point

Consider a neural network whose R_k is based on activations of a_j in the previous layer and computed by :

$$R_k = \max \left(0, \sum_j a_j w_{jk} + b_k \right), \quad (3.48)$$

where $b_k \leq 0$.

To find the root point \tilde{a}_j , one can see that there are 2 cases to be analyzed, namely $R_k = 0$ and $R_k > 0$. For $R_k = 0$, a_j is already the root point. For the latter, the root point can be found by performing line search in some direction \mathbf{v}_j and magnitude t .

$$\tilde{a}_j = a_j - tv_j, \quad (3.49)$$

More precisely, the root point is the intersection point between (3.48) and (3.49) where $R_k = 0$. Hence,

$$0 = \sum_j (a_j - tv_j) w_{jk} + b_k \quad (3.50)$$

$$t \sum_j v_j w_{jk} = R_k \quad (3.51)$$

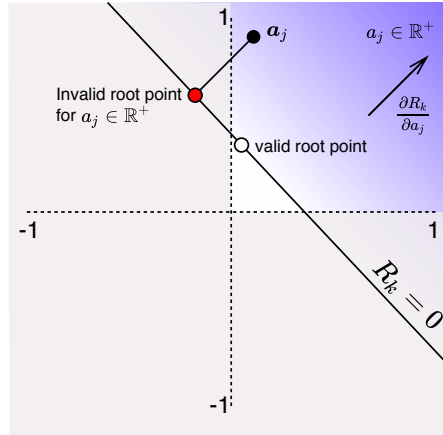
$$t = \frac{R_k}{\sum_j v_j w_{jk}} \quad (3.52)$$

Combining Therefore, R_j can be computed by :

$$R_j = \sum_k \frac{\partial R_k}{\partial a_j} \Big|_{a_j = \tilde{a}_j} (a_j - \tilde{a}_j) \quad (3.53)$$

$$= \sum_k w_{jk} t v_j \quad (3.54)$$

$$= \sum_k \frac{v_j w_{jk}}{\sum_j v_j w_{jk}} R_k \quad (3.55)$$

Figure 3.11: Function's view of R_k and root point candidates

The last step is to find \mathbf{v}_j such that $\tilde{\mathbf{a}}_j$ is the closest point in the same domain as \mathbf{a}_j to the line $R_k = 0$. Figure 3.11 visualizes the intuition. Here, if $a_j \in \mathbb{R}^+$, then \tilde{a}_j must be also in \mathbb{R}^+ . Therefore, \mathbf{v}_j needs to be separately derived for each possible domain.

Case $a_j \in \mathbb{R}$: w^2 -rule

Trivially, the search direction v_j is just the direction of gradient $\frac{\partial R_k^{(l+1)}}{\partial a_j^{(l)}}$:

$$v_j = w_{jk}$$

Hence,

$$R_j = \sum_k \frac{w_{jk}^2}{\sum_j w_{jk}^2} R_k$$

Case $a_j \in \mathbb{R}^+$: z^+ -rule

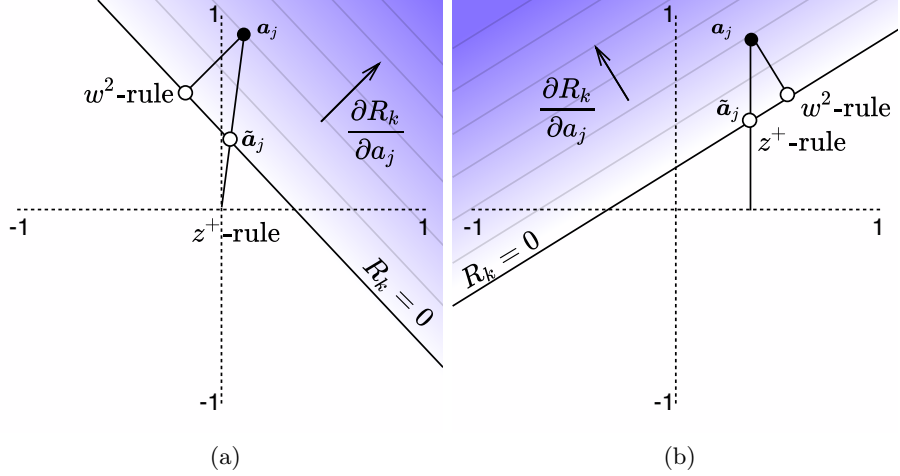
The root point is on the line segment $(a_j \mathbb{1}[w_{jk} < 0], a_j)$. In particular, as shown on Figure 3.12, R_k has a root at $a_j \mathbb{1}[w_{jk} < 0]$, because of:

$$R_k = \max \left(\sum_j a_j w_{jk} + b_k, 0 \right) \quad (3.56)$$

$$= \max \left(\sum_j a_j \mathbb{1}[w_{jk} < 0] w_{jk} + b_k, 0 \right) \quad (3.57)$$

$$= \max \left(\sum_j a_j w_{jk}^- + b_k, 0 \right) \quad (3.58)$$

$$= 0 \quad (3.59)$$

Figure 3.12: Function's view of R_k and the root point from z^+ -rule

The last step uses the fact that $a_j \in R^+$ and $b_k \leq 0$ from the assumption. Hence, the search direction is:

$$v_j = a_j - a_j \mathbb{1}[w_{jk} < 0] \quad (3.60)$$

$$= a_j \mathbb{1}[w_{jk} \geq 0] \quad (3.61)$$

Therefore,

$$R_j = \sum_k \frac{w_{jk} a_j \mathbb{1}[w_{jk} \geq 0]}{\sum_j w_{jk} a_j \mathbb{1}[w_{jk} \geq 0]} R_k \quad (3.62)$$

$$= \sum_k \frac{a_j w_{jk}^+}{\sum_j a_j w_{jk}^+} R_k \quad (3.63)$$

This results the propagation rule that is equivalent to LRP- $\alpha_1\beta_0$.

Case $a_j \in [l_j, h_j]$ **where** $l_j \leq 0 < h_j$: z^β -rule

This situation associates to the first layer where the input is bounded, for example pixel intensity. In this case, as shown in Figure 3.13, the root point is on the line segment $(l_j \mathbb{1}[w_{jk} \geq 0] + h_j \mathbb{1}[w_{jk} \leq 0], a_j)$. In particular, the root point is at $l_j \mathbb{1}[w_{jk} \geq 0] + h_j \mathbb{1}[w_{jk} \leq 0]$.

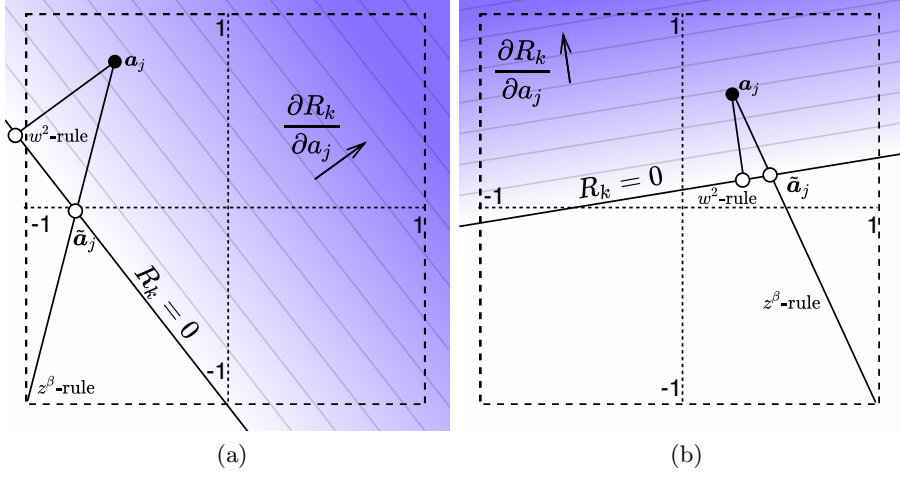


Figure 3.13: Function's view of R_k and the root point from z^β -rule with $-1 < a_j < 1$

$$0] + h_j \mathbb{1}[w_{jk} \leq 0],$$

$$R_k = \max \left(\sum_j a_j w_{jk} + b_k, 0 \right) \quad (3.64)$$

$$= \max \left(\sum_j (l_j \mathbb{1}[w_{jk} \geq 0] + h_j \mathbb{1}[w_{jk} \leq 0]) w_{jk} + b_k, 0 \right) \quad (3.65)$$

$$= \max \left(\sum_j l_j w_{jk}^+ + h_j w_{jk}^- + b_k, 0 \right) \quad (3.66)$$

$$= 0 \quad (3.67)$$

Hence, the search direction is

$$v_j = a_j - \tilde{a}_j \quad (3.68)$$

$$= a_j - l_j \mathbb{1}[w_{jk} \geq 0] - h_j \mathbb{1}[w_{jk} \leq 0] \quad (3.69)$$

Therefore,

$$R_j = \sum_k \frac{w_{jk}(a_j - l_j \mathbb{1}[w_{jk} \geq 0] - h_j \mathbb{1}[w_{jk} \leq 0])}{\sum_j w_{jk}(a_j - l_j \mathbb{1}[w_{jk} \geq 0] - h_j \mathbb{1}[w_{jk} \leq 0])} R_k \quad (3.70)$$

$$= \sum_k \frac{a_j w_{jk} - l_j w_{jk}^- - h_j w_{jk}^+}{\sum_j a_j w_{jk} - l_j w_{jk}^- - h_j w_{jk}^+} R_k \quad (3.71)$$

Table 3.1 concludes the details when each DTD rule should be applied. As a result, the relevance scores, $f(\mathbf{x})$, can be propagated through the network using LRP Algorithm 1.

Rule and input domain	Formula
w^2 -rule : Real values, $a_j \in \mathbb{R}$	$R_j = \sum_k \frac{w_{jk}^2}{\sum_j w_{jk}^2} R_k$
z^+ -rule : ReLU activations, $a_j \in \mathbb{R}^+$	$R_j = \sum_k \frac{a_j w_{jk}^+}{\sum_j a_j w_{jk}^+} R_k$
z^β -rule : Pixel Intensities, $a_j \in [l_j, h_j]$ where $l_j \leq 0 < h_j$	$R_j = \sum_k \frac{a_j w_{jk} - l_j w_{jk}^- - h_j w_{jk}^+}{\sum_j a_j w_{jk} - l_j w_{jk}^- - h_j w_{jk}^+} R_k$

Table 3.1: Relevance propagation rules of deep Taylor decomposition.

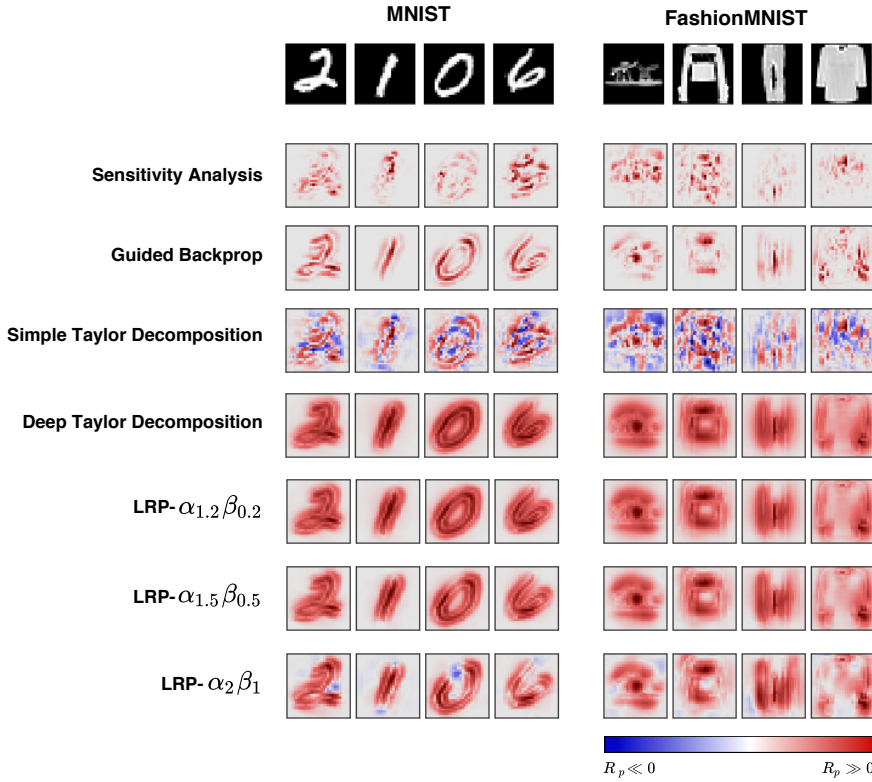


Figure 3.14: Relevance heatmaps from LeNet-5 architecture explained by different explanation methods. Blue indicates negative relevance, while red indicates positive relevance.

In this section, we have described several explanation methods as well as their intuition. Figure 3.14 shows examples of relevance heatmaps from those methods applied on LeNet-5[LeCun et al., 2001] to explain classification decisions that the network makes. The network was trained on 100 epochs with batch size 50 and dropout probability at 0.2. It achieves accuracy at 99.21% for MNIST and 87.90% for FashionMNIST. From the figure, we can also see characteristics of each method. In particular, one can observe that simple Taylor decomposition provides the most noisy and non informative heatmaps, while explanations from sensitivity analysis(SA) also looks noisy but input features can be seen. Guided backprop(GB) produces smoother version of SA heatmaps. On the other hand, explanations from deep Taylor decomposition(DTD) and LRP are more diffuse and smoother than the others : they also look similar when β is small. Given this result, we are going to consider only SA, GB, DTD and LRP- $\alpha_{1.5}\beta_{0.5}$ in experiments.

4 Experiments

4.1 General Setting

We use *Adaptive Moment Estimation(Adam)*[Kingma and Ba, 2014] to train models and initialize weights $w_{ij} \in \mathbf{W}$ and biases $b_j \in \mathbf{b}$ as follows:

$$w_{ij} \sim \Psi(\mu, \sigma, [-2\sigma, 2\sigma])$$

$$b_j = \ln(e^{0.01} - 1)$$

where $\Psi(\cdot)$ denotes Truncated Normal Distribution where $\mathbb{P}(|w_{ij}| > 2\sigma) = 0$. Precisely, we use $\mu = 0$ and $\sigma = 1/\sqrt{|\mathbf{a}|}$ where $|\mathbf{a}|$ is a number of neurons in previous layer.

The activations of neurons in layer j , denoted as $\mathbf{a}^{(j)}$, are computed using :

$$\mathbf{h}^{(j)} = (\mathbf{W}_{i \rightarrow j})^T \mathbf{a}^{(i)} - \sigma_s(\mathbf{b}_j)$$

$$\mathbf{a}^{(j)} = \sigma_r(\mathbf{h}^{(j)})$$

where $\sigma_r(\cdot)$ and $\sigma_s(\cdot)$ are *ReLU* and *softplus* function respectively and applied element-wise to the vectors.

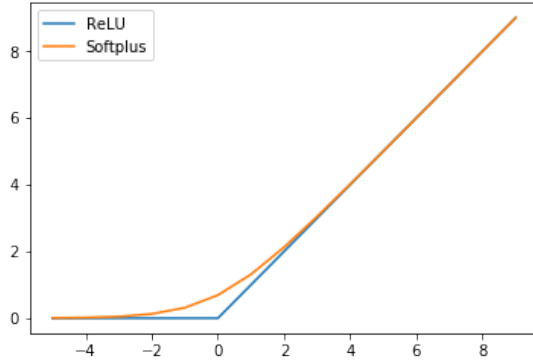


Figure 4.1: ReLU and Softplus function

The reason of using softplus function for the bias term is due to the non positive bias assumption of DTD. Moreover, because of the continuity of softplus function, bias term can be more flexibly adjusted through back-propagation than using ReLU. With this setting, the initial value of bias term $\sigma_s(b_j)$ is then 0.01.

Dropout technique [Srivastava et al., 2014] is applied to activations of every fully-connected layer, unless stated otherwise, with the probability at 0.2. We train models

Hyperparameter	Value
Optimizer	Adam
Epoch	100
Dropout Probability	0.2
Batch size	50

Table 4.1: Summary of hyperparameter.

Dataset	Minimum Accuracy
MNIST	98.00%
FashionMNIST	85.00%

Table 4.2: Minimum classification accuracy for models to be considered.

with batch size 50 for 100 epochs. Table 4.1 summaries the setting of hyperparameters. On the other hand, Learning rate is not globally fixed and left adjustable per architecture: the value varies between 0.0001 and 0.0005. Based on literature surveys, Table 4.2 shows minimum accuracy for models to be used in the following experiments. Numbers of neurons in each layer were carefully chosen such that every architecture has similar number of trainable variables. More precise configuration will be discussed separately in each experiment.

Denote g_r and g_f function that a RNN with $\theta = \{\mathbf{W}, \mathbf{b}\}$ uses to compute recurrent input \mathbf{r}_{t+1} and $f(\mathbf{x})$ respectively. For a classification problem with K classes, the calculations can be roughly summarized as follows:

$$\begin{aligned} \mathbf{r}_{t+1} &= g_r(\theta, \mathbf{x}_t, \mathbf{r}_t) \\ &\vdots \\ f(\mathbf{x}) &= g_f(\theta, \mathbf{x}_T, \mathbf{r}_T) \\ \hat{\mathbf{y}} &= \text{softmax}(f(\mathbf{x})), \end{aligned}$$

where $t \in \{1, \dots, T\}$, $(\mathbf{x}_t \in \mathbf{x})_1^T$ are the input corresponding to step t , $\mathbf{r}_0 = \mathbf{0}$, and $\hat{\mathbf{y}} \in \mathbb{R}^K$ are the class probabilities. To compute explanation or relevance heatmap of \mathbf{x} , denoted as $R(\mathbf{x})$, we take $z^* \in f(\mathbf{x})$ that is corresponding to the true target class, instead of the predicted class. Because DTD and LRP method are primarily based on distributing positive relevance, we also introduce a constant input to softmax function with value zero to force building positive relevance, $z^* \in \mathbb{R}^+$. Mathematically, this constant does not affect the training procedure.

Our implementation is written in Python and TensorFlow[Abadi et al., 2016]. It is also publicly available on Github¹. We run our experiments either on a GeForce GTX 1080 provided by TUB ML group or AWS’s p2.xlarge² instance. It approximately takes

¹<https://github.com/heytitle/thesis-designing-recurrent-neural-networks-for-explainability/releases/tag/release-final>

²<https://aws.amazon.com/ec2/instance-types/p2/>

2 hour to train a model.

4.2 Experiment 1 : Sequence Classification

4.2.1 Problem Formulation

We consider this experiment as a preliminary study. Here, we constructed an artificial classification problem in which each image sample \mathbf{x} is column-wise split into a sequence of non-overlapping $(\mathbf{x}_t)_{t=1}^T$. The RNN classifier needs to summarize information from the sequence $(\mathbf{x}_t)_{t=1}^T$ to answer what is the class of \mathbf{x} . Using image allows us to conveniently inspect how well RNNs can distribute relevant quantities to input space.

Figure 4.2 illustrates the setting. Here, a MNIST sample $\mathbf{x} \in \mathbb{R}^{28,28}$ is divided to a sequence of $(\mathbf{x}_t \in \mathbb{R}^{28,7})_{t=1}^4$. At time step t , \mathbf{x}_t is presented to the RNN classifier yielding recurrent input r_{t+1} for the next step. For the last step T , in this example $T = 4$, the RNN classifier computes $f(\mathbf{x}) \in \mathbb{R}^{10}$ and class probabilities accordingly.

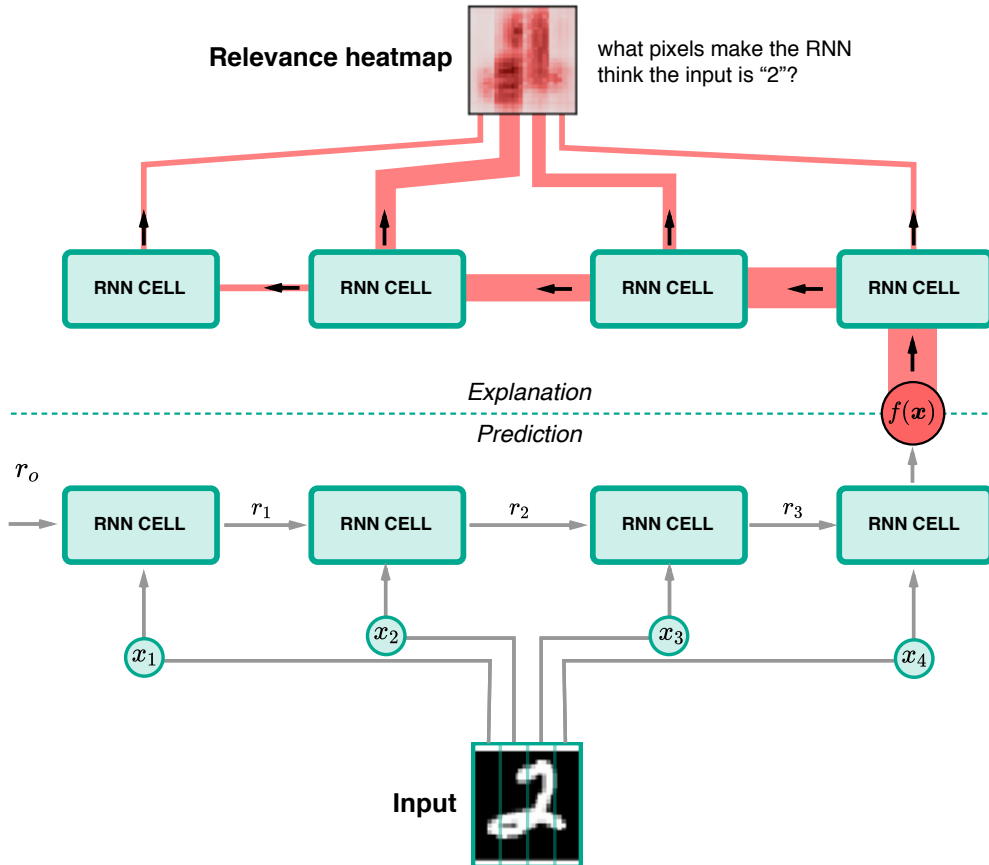


Figure 4.2: RNN Sequence classifier and decision explanation

We are considering to 2 cell architectures in this experiment, namely

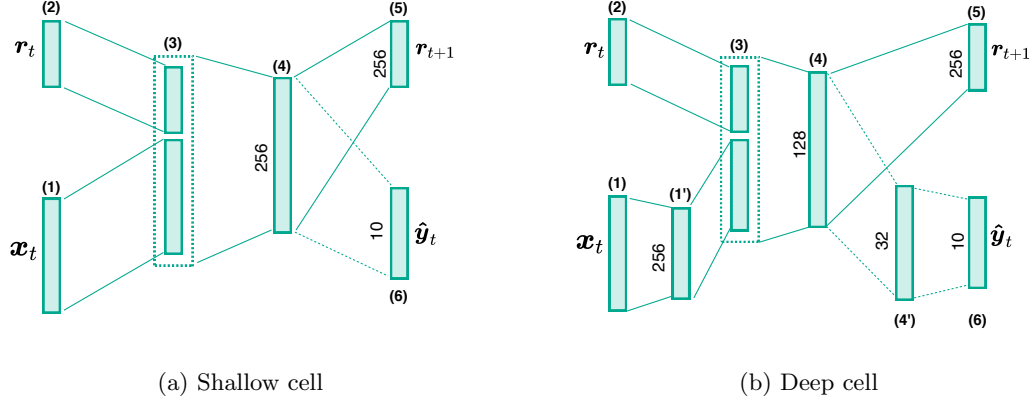


Figure 4.3: Shallow and Deep cell architecture with number of neurons at each layer depicted.

1. Shallow cell

As shown in Figure 4.3a, the Shallow cell first concatenates input \mathbf{x}_t and recurrent input \mathbf{r}_t at layer (3) as one vector before computing activations of layer (4), denoted as $\mathbf{a}_t^{(4)}$. Then, the next recurrent input \mathbf{r}_{t+1} (5) is derived from $\mathbf{a}_t^{(4)}$. In the last step T , $f(\mathbf{x})$ is computed from $\mathbf{a}_T^{(4)}$ and applied to softmax function to compute class probabilities $\hat{\mathbf{y}}$. **TODO : Adpated LRP rules for mixed domain propagation**

2. Deep cell

Figure 4.3b illustrates the architecture of the Deep cell. Unlike the Shallow architecture, the Deep cell has 2 more layers, namely (1') and (4'). The idea is to let (1') learn representations of the input, while (4) can focus on combining information from the past and current input. This then enables (4') to compute more fine-grained decision probabilities.

		No. trainable variables	
T	Dim. of \mathbf{x}_t	Shallow	Deep
1	$\mathbb{R}^{28,28}$	269,322	271,338
4	$\mathbb{R}^{28,7}$	184,330	153,578
7	$\mathbb{R}^{28,4}$	162,826	132,074

Table 4.3: Dimensions of \mathbf{x}_t and number of trainable variables in each cell architecture on sequence length $T = \{1, 4, 7\}$.

We experimented with MNIST and FashionMNIST data using sequence length $T =$

T	MNIST		FashionMNIST	
	Shallow	Deep	Shallow	Deep
1	98.11%	98.22%	87.93%	89.14%
4	98.56%	98.63%	89.04%	89.43%
7	98.66%	98.68%	89.28%	88.96%

Table 4.4: Accuracy of models trained for sequence classification problem with different sequence lengths and dataset.

$\{1, 4, 7\}$. Table 4.3 shows dimensions of \mathbf{x}_t for different sequence length as well as number of trainable variable in each architecture.

To simplify the writing, we are going to use *ARCHITECTURE- T* convention to denote a RNN with *ARCHITECTURE* trained on the sequence length T . For example, Deep-7 refers to the Deep cell trained on $(\mathbf{x}_t \in \mathbb{R}^{28,4})_{t=1}^7$.

4.2.2 Result

Table 4.4 summarizes accuracy of the trained models. Both Shallow and Deep architecture have comparable accuracy, hence their explanations can also be compared. Figure 4.4 shows relevance heatmaps from Shallow and Deep architecture trained on MNIST. We can observe general characteristics of each explanation technique. In particular, sensitivity analysis(SA) and guided backprop(GB) heatmaps are sparse, while the ones from deep Taylor decomposition(DTD) and Layer-Wise Relevance Propagation (LRP) are more diffuse throughout \mathbf{x} .

When applying these techniques to Shallow-1 and Deep-1, the relevance heatmaps look similar regardless of the architectures. As the sequence length is increased, SA and GB heatmaps are still almost identical for Shallow-4 and Deep-4 as well as their 7-sequence length pair. However, this is not the case for DTD and LRP. From the figure, we can see that Shallow-4,7 and Deep-4,7 produce significantly different relevance heatmaps when being explained by DTD and LRP- $\alpha_{1.5}\beta_{0.5}$ method. In particular, Shallow-4,7's heatmaps are mainly concentrated on the right part of \mathbf{x} associating to last time steps, while Deep-4,7's ones are proportionally highlighted around content area of \mathbf{x} .

Relevance heatmaps of Shallow and Deep architecture trained on FashionMNIST are shown on Figure 4.5. Similar to the ones from MNIST, we do not see any remarkable difference on SA and GB heatmaps of the two architectures : only that Deep-4,7 produces slightly more sparse heatmaps than Shallow-4,7. However, the wrong concentration issue of DTD and LRP seems to appear on both Shallow-4,7's and Deep-4,7's heatmaps. Nevertheless, we can still observe proper highlight from Deep architecture on some samples. For example, the trouser sample, we can see that Deep-4,7 architecture manage to distribute high relevance scores to area of the trouser.

Similar structures of FashionMNIST samples might be one of the reasons why Deep

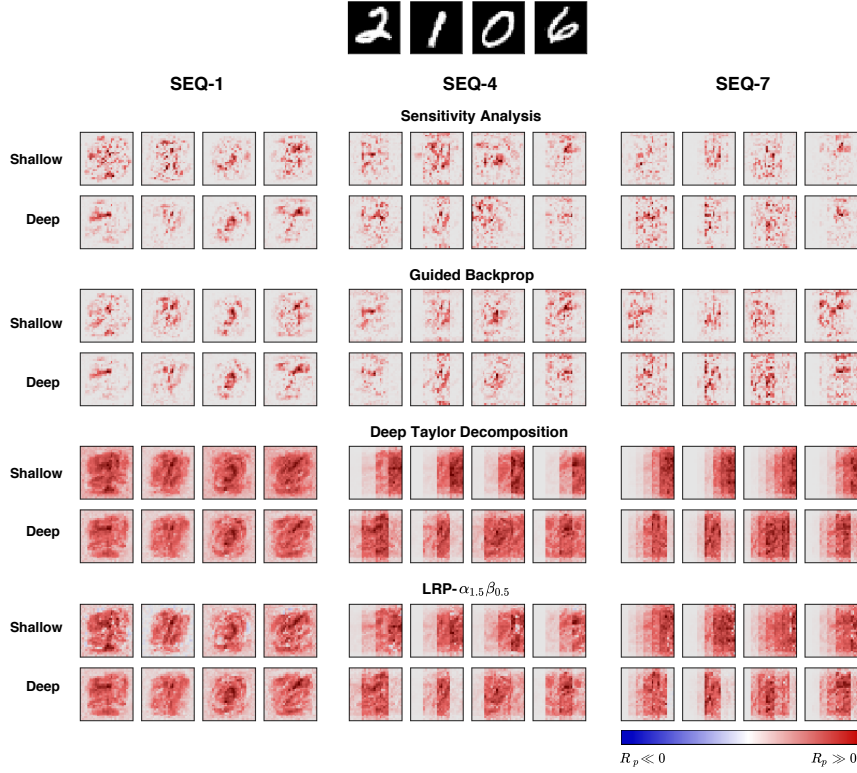


Figure 4.4: Relevance heatmaps from different explanation techniques applied to Shallow and Deep architecture trained on MNIST with different sequence lengths. Blue indicates negative relevance, while red indicates positive relevance.

architecture is not able to distribute relevance scores to earlier steps as in MNIST cases. Consider *Shoe* and *Ankle Boot* samples in Figure 1.2. One can see that their front part are similar and only the heel part that determines the differences between the two categories. This evidence suggests that more robust feature extractor layer, such as convolution and pooling layer, might be more suitable than the fully-connected one.

Figure 4.6 presents relevance heatmaps of MNIST *Class 1* and FashionMNIST *Class Trouser* samples. These samples were chosen to emphasize the impact of RNN architecture on DTD and LRP explanation. In particular, as can be seen from the figure, these samples have \mathbf{x}_t' containing actual content primarily locating at the center, or middle of the sequence. Hence, relevance heatmaps should be highlighted at \mathbf{x}_t' and possibly its neighbors. As expected, we can see Deep-7 produces sound explanations in which the heatmaps have high intensity value where \mathbf{x}_t' approximately locate, while Shallow-7 mainly assigns relevance quantities to \mathbf{x}_t for $t \approx T$.

Figure 4.7 further shows a quantitative evidence of this wrong propagation issue of DTD and LRP- $\alpha_{1.5}\beta_{0.5}$. Here, distributions of relevance scores derived by the methods from Shallow-7 and Deep-7 are plotted across time step $t = \{1, \dots, 7\}$. The distributions are

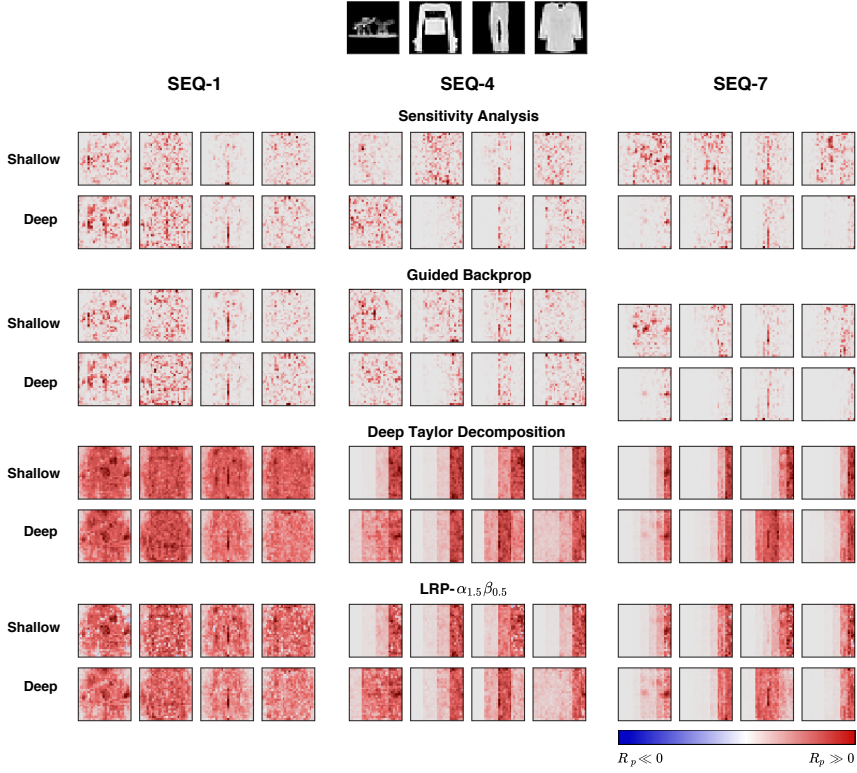


Figure 4.5: Relevance heatmaps from different explanation techniques applied to Shallow and Deep architecture trained on FashionMNIST with different sequence lengths. Blue indicates negative relevance, while red indicates positive relevance.

computed from all test samples in MNIST *Class 1* and FashionMNIST *Class Trouser* respectively. The plots also include distribution of pixel intensity values. We can see that the relevance distributions from Deep-7 align with the data distributions, while the distributions from Shallow-7 ones diverge with significant margin. Approximately, one can see that Shallow-7 distributes more than 90% of relevance scores to the last 3 steps, namely x_5 , x_6 and x_7 .

4.2.3 Summary

TODO : review Results from this first experiment seem to suggest that choice of RNN architectures has an impact on quality of its explanation. In particular, as presented in Figure 4.6 and Figure 4.7, quality of deep Taylor decomposition(DTD) explanation is significantly influenced by the architecture. In contrast, we do see such notable effect from sensitivity analysis(SA) and guided backprop(GB) method. In the following experiment, I am going to present a methodical evaluation of this impact in detail.

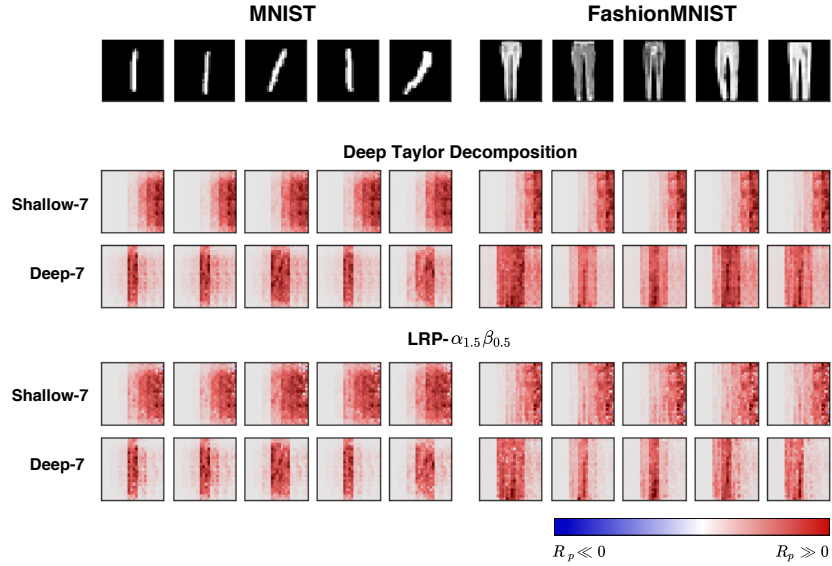


Figure 4.6: Relevance heatmaps of MNIST *Class 1* and FashionMNIST *Class Trouser* samples from Shallow-7 and Deep-7 explained by DTD and LRP- $\alpha_{1.5}\beta_{0.5}$. Blue indicates negative relevance, while red indicates positive relevance.

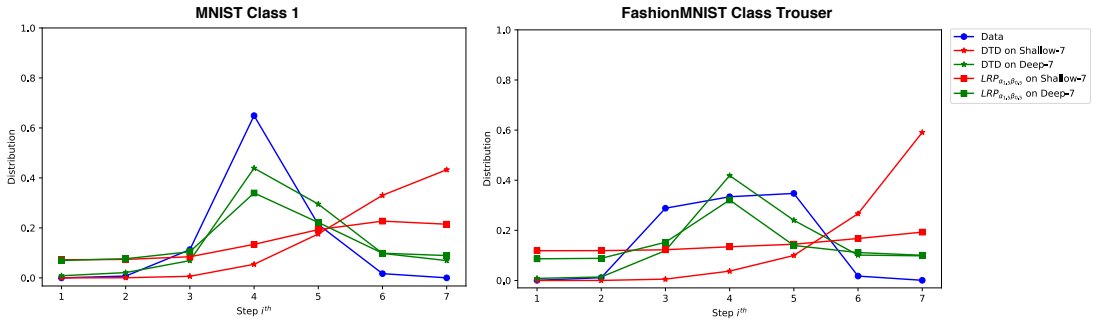


Figure 4.7: Distribution of pixel intensity, relevance quantities from Shallow-7 and Deep-7 propagated by DTD and LRP- $\alpha_{1.5}\beta_{0.5}$ and averaged over MNIST *Class 1* and FashionMNIST *Class Trouser* test population.

4.3 Experiment 2 : Majority Sample Sequence Classification

4.3.1 Problem Formulation

When neural networks are trained, one can apply explantation techniques to the models to get relevance heatmaps of samples. The heatmap of sample x illustrates important features in x that the trained network utilizes to perform its objective prediction, such as classification. Therefore, one needs to know the ground truth of these latent features in order to methodologically evaluate how well the model distributes relevance scores

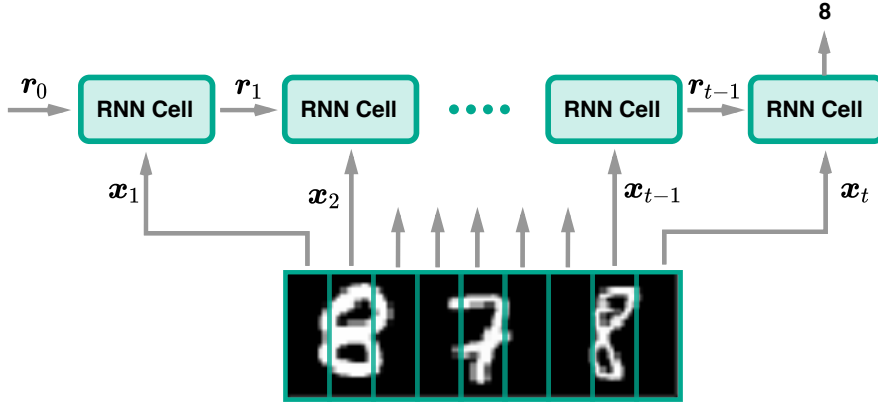


Figure 4.8: Majority Sample Sequence Classification(MAJ) problem.

to the input space, in other words, how the model can be explained. However, this knowledge is not trivial to find as it is an incident from the optimization process in high-dimensional space that we in fact seek to understand.

To alleviate this challenge, we instead constructed another artificial classification problem where RNNs are trained to classify the majority group in a sequence \mathbf{x} , $(\mathbf{x}_t)_{t=1}^T$. Consider MNIST. \mathbf{x} is constructed as follows: each original sample $\tilde{\mathbf{x}} \in \mathbb{R}^{28,28}$, we randomly selected 2 additional samples : one from the same class of $\tilde{\mathbf{x}}$ and the other one from a different class. Then, these 3 samples are concatenated in random order yielding a sample $\mathbf{x} \in \mathbb{R}^{28,84}$. Figure 4.8 illustrates the construction and the objective classification. Given $\mathbf{x} = \{8, 7, 8\}$, the classification result is “8”. We call this problem as MNIST-MAJ when \mathbf{x} are constructed from MNIST samples and the same for FashionMNIST-MAJ.

By construction, we already know blocks of digit/item that belong to the majority group. More precisely, we know time step t' that are parts of those blocks, hence, we can use this information to quantitatively evaluate how well RNN architectures can propagate relevance quantities to the input, in other words, how well they can be explained.

As discussed in the previous experiment that some DTD and LRP- $\alpha_{1.5}\beta_{0.5}$ heatmaps from the Deep architecture were not as good as the others. This seems to suggest that the architecture might not have enough capability to extract proper representations from FashionMNIST samples, causing the incorrect propagation issue on such heatmaps.

Hence, apart of Shallow and Deep architecture, we also introduced another two architectures, namely DeepV2 and ConvDeep. The DeepV2 cell has one more layer after the first fully-connected layer than the Deep cell. On the other hand, the ConvDeep cell instead employs a sequence of convolutional and pooling operation and a fully-connected layer between the input layer and the internal layer. Figure 4.9 shows details of the new architectures.

Lastly, despite the fact that our implementation is readily to apply on different sequence lengths, we conducted the experiment with only sequence length $T = 12$, or

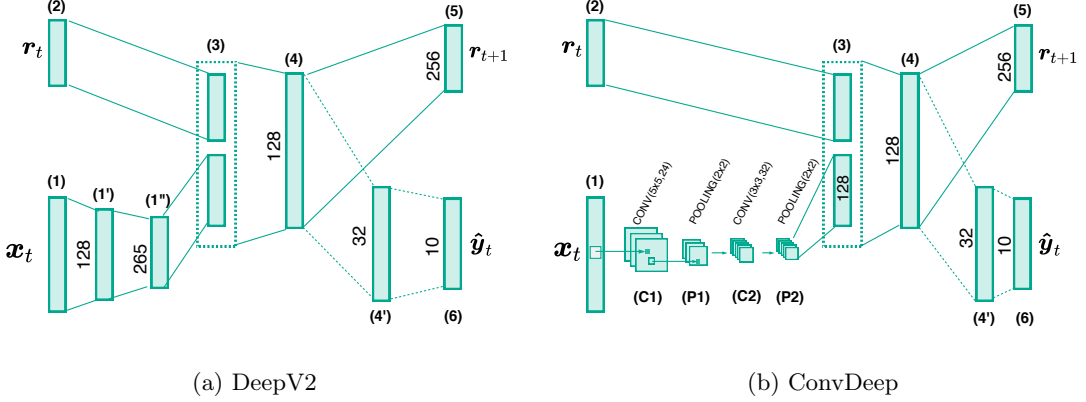


Figure 4.9: DeepV2 and ConvDeep cell architecture with number of neurons at each layer depicted.

$(x_t \in \mathbb{R}^{28,7})_{t=1}^{12}$. This is mainly due to computational resources and time constraint we had. Consequently, slightly abusing the name convention proposed in Section 4.2, we are going to write only the name of architecture without explicitly stating the sequence length towards the end of this chapter.

4.3.2 Evaluation Methodology

From the problem construction, we know that relevance quantities should be primarily assigned to blocks that belong to the majority group. This construction enables us to both directly examine quality of produced relevance heatmaps visually as well as quantitative evaluation. In particular, for qualitative inspections, we constructed training and testing data based on the original training and testing split that [LeCun and Cortes, 2010] and [Xiao et al., 2017] proposed and trained with setting described in Section 4.1. **TODO : talk about ability to distributed relevance to reight region and visual perception**

Quantitative Evaluation

A straightforward way to quantitatively evaluate results is to calculate proportion of relevance distributed to pixels that are contained in the blocks of the majority group digit/item. However, this measurement has a shortcoming where architectures can achieve high score if they distribute relevance to only one of the correct blocks. Hence, we then propose to use *cosine similarity* instead. The cosine similarity is computed from a binary vector $\mathbf{m} \in \mathbb{R}^3$ whose values represent correctness of the blocks and a vector $\mathbf{v} \in \mathbb{R}^3$ of relevance percentage distributed to the blocks.

$$\cos(\mathbf{m}, \mathbf{v}) = \frac{\mathbf{m} \cdot \mathbf{v}}{\|\mathbf{m}\|_2 \|\mathbf{v}\|_2} \quad (4.1)$$

As illustrated in Figure 4.10, the percentage of correctly distributed relevance can be significantly high although the relevance heatmap does not show any highlight at the left most block of “0”. Therefore, using cosine similarity is more reasonable. In fact, the propagation needs to be equally balanced between the two blocks in order to achieve the highest score, “1”. For LRP- $\alpha_{1.5}\beta_{0.5}$ heatmaps, we ignore negative relevance and set it to zero before computing cosine similarity.

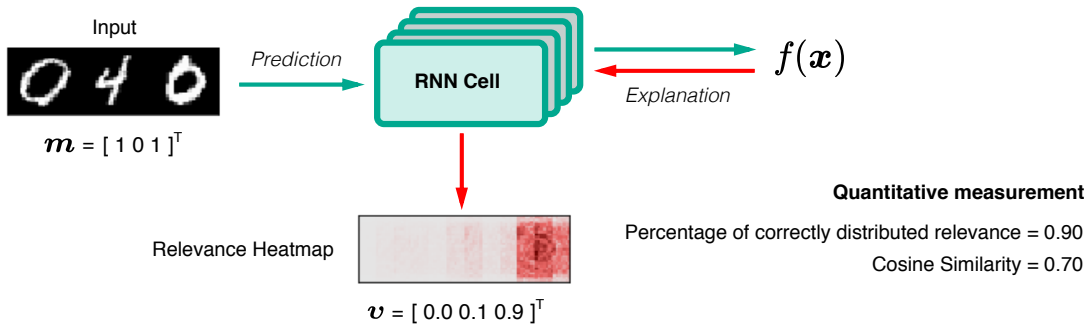


Figure 4.10: Comparison between percentage of correctly distributed relevance and cosine similarity.

Statistical Evaluation

To reduce variations possibly introduced by, for example variable initialization, we conducted quantitatively evaluations through k -fold cross-validation where we combined training and testing set together before splitting into k folds. Each fold is used as the testing set once. For each cross-validation iteration, we average the cosine similarity across testing samples. The final result is then averaged from folds' statistics. To keep the same proportion of training and testing data, we chose $k = 7$.

TODO : hypo : check whether we need it: It is also possible that some architectures might perform similarly and the difference is not visually observed. For such scenarios, we will use one-way ANOVA on statistics of cosine similarity and pairwise Tukey Honest Significant Difference (HSD) as a post-hoc test to verify whether there are statistically significant results. We use significance level at 0.05. Dataset is considered as a confounding variable. This procedure is conducted separately for each explanation method.

4.3.3 Result

Table 4.5 shows number of trainable variables and accuracy of the trained models. These trained models have equivalent number of variables and accuracy, hence comparing heatmaps of these models is a fair evaluation.

Figure 4.11 shows that the deeper architecture improves relevance propagation, or easier to be explained. In particular, we can see that fewer relevant scores distributed

Cell architecture	No. variables	Accuracy	
		MNIST-MAJ	FashionMNIST-MAJ
Shallow	184,330	98.12%	90.00%
Deep	153,578	98.16%	89.81%
DeepV2	161,386	98.26%	90.57%
ConvDeep	151,802	99.22%	92.87%

Table 4.5: Number of trainable variables and model accuracy from architectures trained on MNIST-MAJ and FashionMNIST-MAJ with sequence length $T = 12$.

to irrelevant region are gradually reduced from Shallow to ConvDeep architecture. This effect happens across all explanation methods. This result further supports the evidence discussed in Section 4.2. Moreover, although relevance heatmaps from Shallow, Deep, and DeepV2 generally look noisy, increasing the depth of architecture seems to reduce the noise in the heatmaps as well. On the other hand, ConvDeep does not only properly assign relevance quantities to the right time steps, but its heatmaps contains \mathbf{x} 's features that we can not easily observe from the other architectures. For example, GB and LRP- $\alpha_{1.5}\beta_{0.5}$ heatmaps of Digit 1 and Sandal samples are cases.

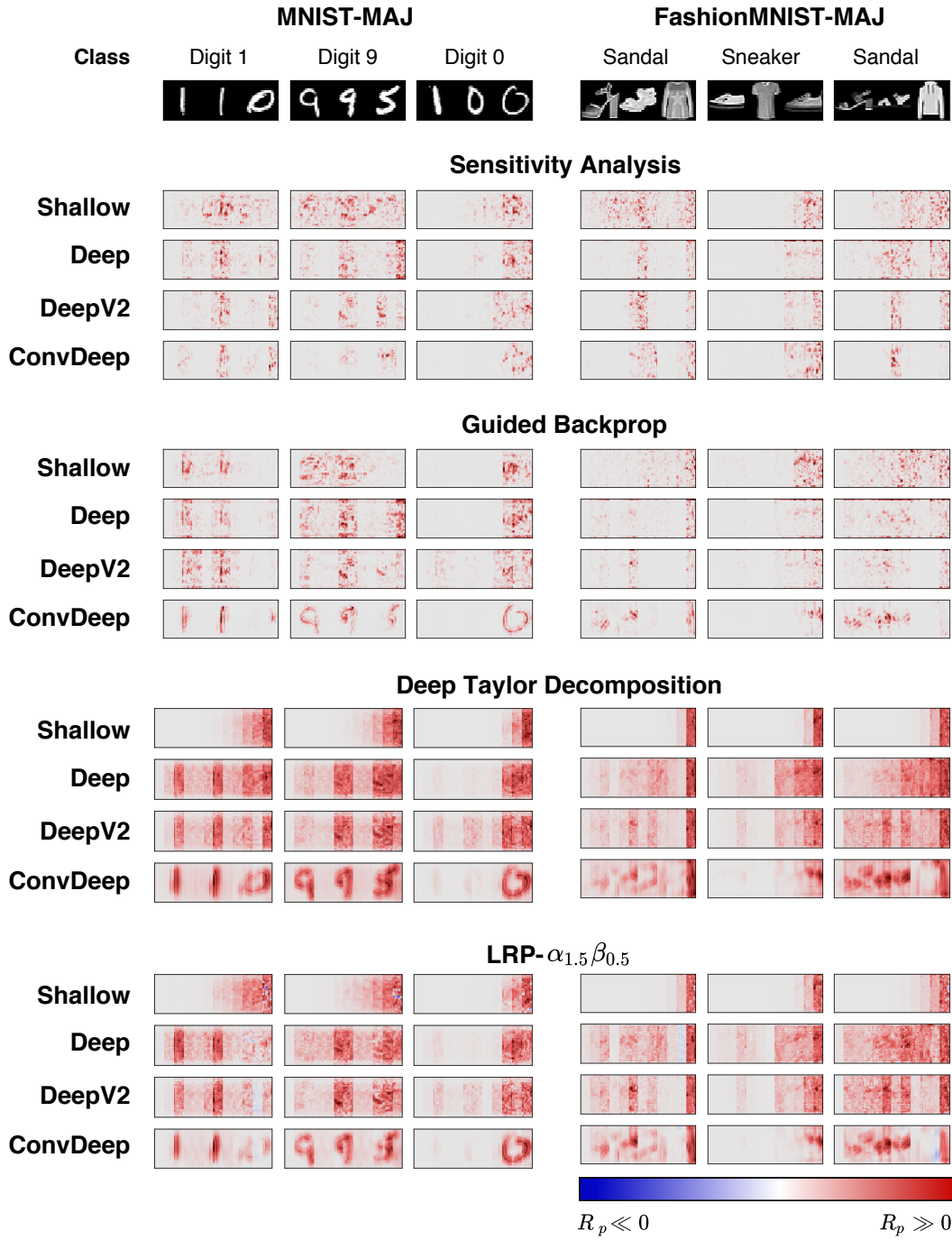


Figure 4.11: Relevance heatmaps from different explanation techniques applied to Shallow, Deep, DeepV2 and ConvDeep architecture trained on MNIST-MAJ and FashionMNIST-MAJ with sequence length $T = 12$. Blue indicates negative relevance, while red indicates positive relevance.

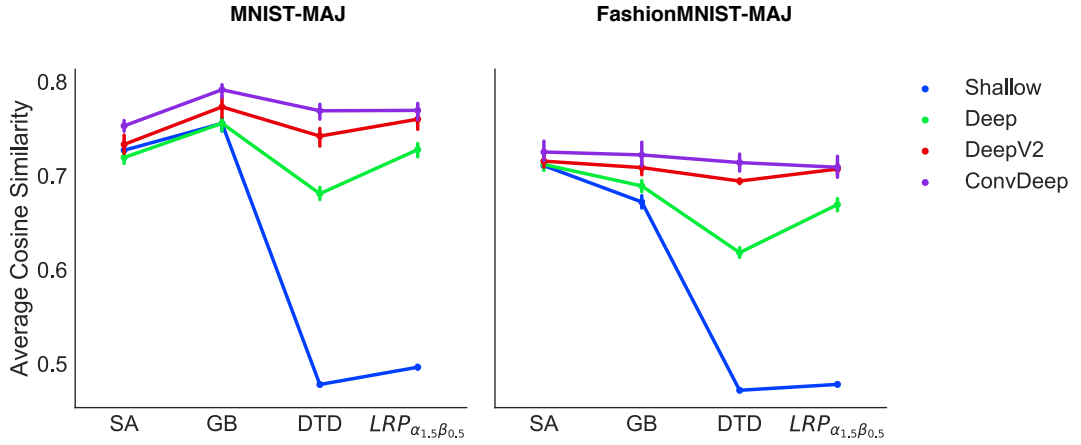


Figure 4.12: Average cosine similarity from different explanation techniques and Shallow, Deep, DeepV2 and ConvDeep architecture. The values are averaged from cross-validation results and the vertical lines depicted 95% confidence interval. The baseline is the Shallow architecture depicted by the blue line. Accuracy of the models can be found at Appendix 1

Figure 4.12 presents a quantitative evaluation of the impact from the depth of architecture to the explanation. The measurement is cosine similarity between a mark vector $\mathbf{m} \in \mathbb{R}^3$ and an aggregated relevance to blocks of digit/item vector $\mathbf{v} \in \mathbb{R}^3$ and averaged through 7-fold cross-validation procedure as described in Section 4.3.2. Results from the figure indicate that the depth of architecture indeed improves quality of the explanations. In particular, the percentage of correct relevance assignment of each explanation technique increases as more layers introduced. This effect can be seen clearly from the result of FashionMNIST-MAJ. Additionally, we can observe that the difference of cosine similarity between the baseline, Shallow, and the other architectures changes with different proposition across methods. In particular, we see the difference from DTD and $LRP_{\alpha_{1.5}\beta_{0.5}}$ are much larger than the other methods. This implies that some explanation methods are more sensitive to architecture configuration than the others.

TODO : hypo : pair wise statistical testing

4.3.4 Summary

The outcome of this experiment quantitatively confirms that the depth of architecture has impacts on explanation of the model. It also shows that the depth of architecture affects explanation in different level on different methods. More precisely, quality of explanations produced by deep Taylor decomposition(DTD) and Layer-Wise Relevance Propagation(LRP) technique are more sensitive to the architecture of the explained model than sensitivity analysis(SA) and guided backprop(GB) method.

Nonetheless, we have also observed that significant amount of relevance scores are distributed to irrelevant regions, for example, consider Digit “9” sample on Figure 4.11.

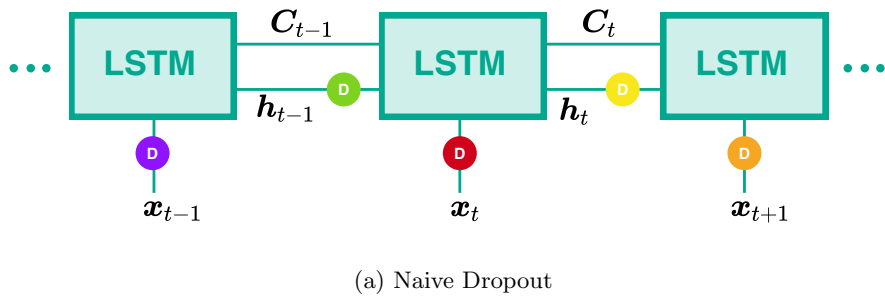
Therefore, we are going to propose several improvements to the problem.

4.4 Experiment 3 : Improve Relevance Propagation

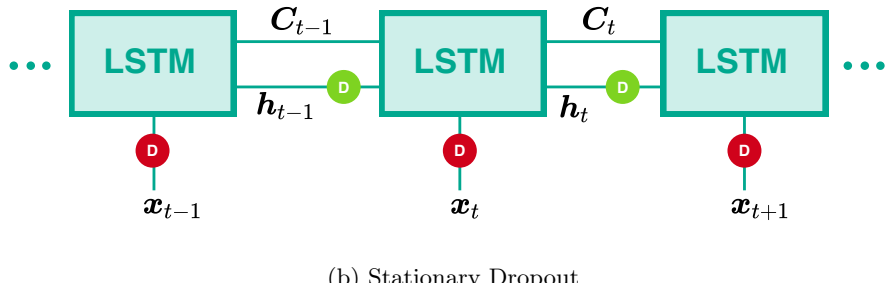
The results from the previous experiment show that better structured cell architecture leads to better explanation, in other words, easier to be explained. However, there are some cases that the proposed architectures fail to distribute relevance properly. Hence, this experiment aims to extend the proposed architectures further to better address the problem. More precisely, we consider the same setting as Section 4.3.1. Here, we propose 3 improvements, namely stationary dropout, employing gating units, and literal connections of convolutional layers.

4.4.1 Proposal 1 : Stationary Dropout

Dropout is a simple regularization technique that randomly suspends activity of neurons during training[Srivastava et al., 2014]. This randomized suspension allows the neurons to learn more specific representations and reduces chance of overfitting. As a result, its influence directly impacts the quality of explanation.



(a) Naive Dropout



(b) Stationary Dropout

Figure 4.13: LSTM with different dropout approaches. \circled{D} indicates a dropout mask and its color represents the suspension activity.

However, unlike typical feedforward architectures, RNN layers are reused across time step, hence a question arises whether the same neurons in those layers should be sus-

pended or they should be different neurons when applying the layers multiple times. Figure 4.13 illustrates these 2 different approaches where different colors represent different dropping activities. In particular, this stationary dropout was first proposed by [Gal and Ghahramani, 2016] who applied the technique to LSTM and GRU and found accuracy improvements on language modeling tasks.

4.4.2 Proposal 2 : Gating units

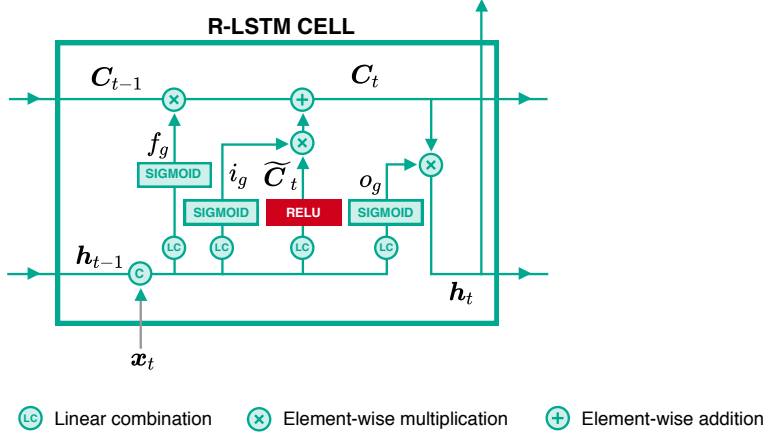


Figure 4.14: R-LSTM Structure

It is already shown that gating units and additive updates are critical mechanisms that enable LSTM to learn long term dependencies [Greff et al., 2017, Jozefowicz et al., 2015]. However, LSTM is not readily applicable for methods we are considering in this thesis. More precisely, the use of sigmoid and tanh activations violates the assumption of GB and DTD. Therefore, we propose a slight modified version of LSTM where ReLU activations are used to compute cell state candidates \tilde{C}_t instead of tanh functions. This results $C_t \in \mathbb{R}^+$, hence the tanh activation for h_t is also removed. Sigmoid activations are treated as constants when applying DTD and LRP, while its gradients are set to zero for GB. We refer this architecture as R-LSTM to differentiate from the original. Figure 4.14 presents an overview of R-LSTM architecture.

4.4.3 Proposal 3 : Convolutional layer with literal connections

As discussed in Section 3.1.3, convolution and pooling operator enable neural networks to learn hierarchical and invariant representations, which are directly beneficial to explanation quality. Because the ConvDeep architecture we proposed in Section 4.3 does not seem to exploit this properly because it has recurrent connections only layers after the convolutional and pooling layers. This can be analogically viewed that the ConvDeep architecture only shares high-level features between step instead of low-level features. This might lead to obscure low-level features in the explanation.

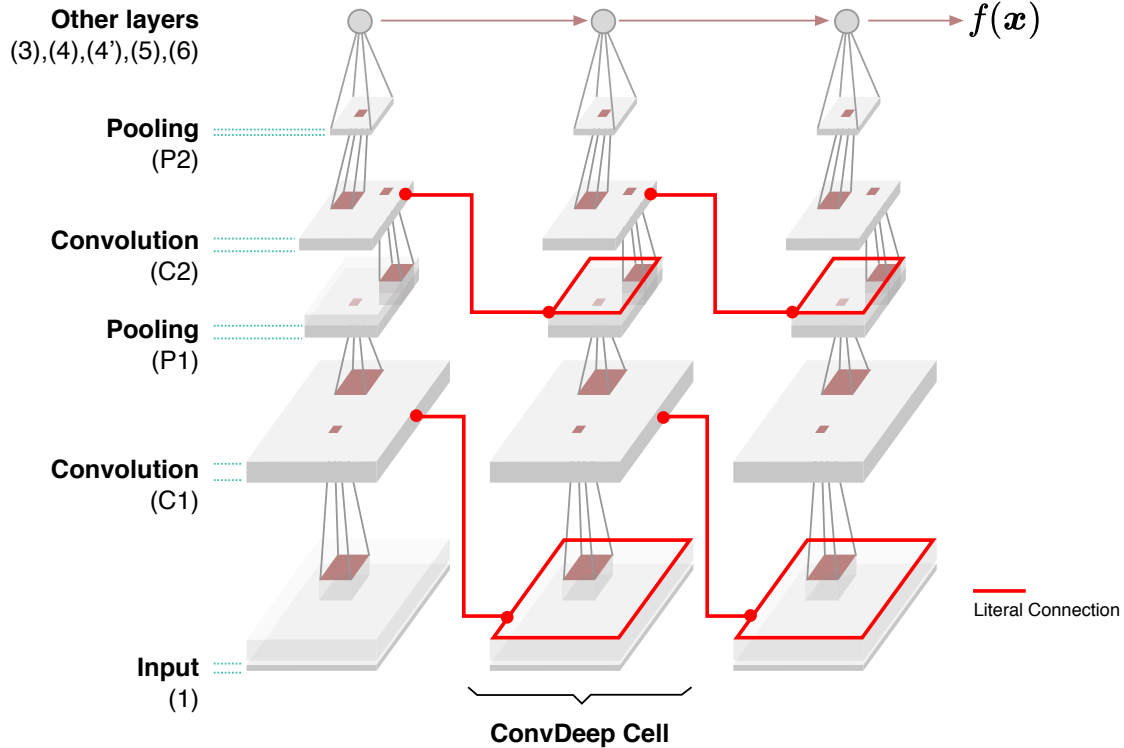


Figure 4.15: ConvDeep with literal connections (Conv⁺Deep).

Therefore, we propose to also share results from convolution operators to the operators in the next step. We name this connections as *literal connections* and Figure 4.15 illustrates such connections in red. From the following, we are going to refer Conv⁺ to the setting where convolutional layers are connected through the literal connections.

In this experiment, we divided results into 2 parts. The first part focuses on stationary dropout and R-LSTM proposal and use the Deep architecture as a baseline. We refer models trained with stationary dropout with $-SD$ suffix. For R-LSTM's configuration, we also added one layer with 256 neurons between the input and 75 R-LSTM cells to make it comparable to the Deep architecture. **TODO : Figure X : show R-LSTM setting**

In the second part, we are going to discuss results from the literal connection proposal as well as results from ConvR-LSTM where the first fully-connected layer is replaced by convolutions and pooling layers with the same configuration as in ConvDeep. The number of R-LSTM cells is also the same to the first part.

TODO : figure describe R-LSTM settings with cell?

4.4.4 Result

Table 4.6 shows number of trainable parameters in the proposed architectures as well as accuracy.

Cell architecture	No. variables	Accuracy	
		MNIST-MAJ	FashionMNIST-MAJ
Deep-SD	153,578	98.10%	89.47%
R-LSTM	145,701	98.50%	91.35%
R-LSTM-SD	145,701	98.57%	91.52%
Conv ⁺ Deep	175,418	97.92%	88.10%
ConvR-LSTM-SD	152,125	99.35%	93.60%
Conv ⁺ R-LSTM-SD	175,741	98.48%	88.19 %

Table 4.6: Number of trainable variables and model accuracy of the proposed architectures for MNIST-MAJ and FashionMNIST-MAJ.

Stationary Dropout and R-LSTM

Figure 4.16 shows results of the first part of this experiment. Here, variants of Deep and R-LSTM are compared. From the figure, it is obvious that R-LSTM provides better explanations than the Deep architecture. More precisely, we can directly observe the improvements from GB, DTD and LRP- $\alpha_{1.5}\beta_{0.5}$ heatmaps. Moreover, training with stationary dropout seems to produce R-LSTM with higher explanation capability. This is well notable on explanations from DTD and LRP- $\alpha_{1.5}\beta_{0.5}$. In contrast, stationary dropout does not seem to have any prominent impact on the Deep architecture.

Figure 4.17 presents the quantitative evaluation. As a reminder, these plots are cosine similarity averaged over models trained with cross validation procedure described in Section 4.3.2. The figure shows that R-LSTM significantly improves relevance distribution than the Deep architecture regardless of explanation techniques. This means that R-LSTM is more explainable than the Deep architecture. Similar to one observation in Section 4.2.2, we also see that the proportion of the improvement of DTD and LRP seem to have greater advantage from R-LSTM than the other methods.

Figure 4.17 also shows another interesting result. We can see that R-LSTM trained with stationary dropout, or R-LSTM-SD, produces better explanations than R-LSTM on FashionMNIST-MAJ, although the difference does not obvious on MNIST-MAJ. This might be due to complexity of FashionMNIST samples' structures, as a result keeping dropout mask the same for all step would enable the network to efficiently learn latent features from homogenous input. In contrast, this does not seem to be the case for the Deep architecture. Particularly, we find that the cosine similarity measurement of Deep-SD is lower than Deep in any case.

TODO : hypo thesis?

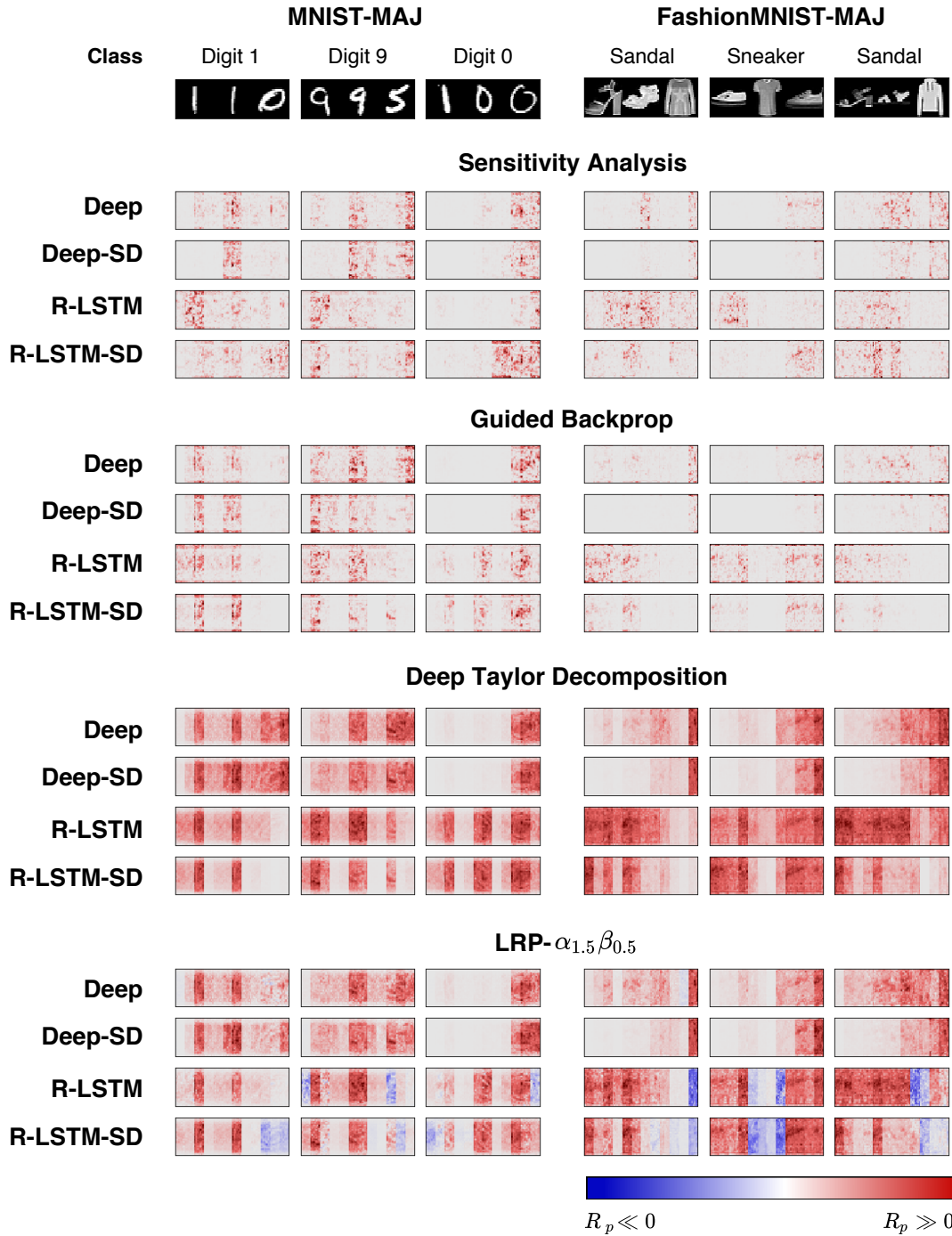


Figure 4.16: Relevance heatmaps produced by different explanation techniques on Deep and R-LSTM architecture trained on MNIST-MAJ and FashionMNIST-MAJ with sequence length $T = 12$ and different dropout configurations. Blue indicates negative relevance, while red indicates positive relevance.

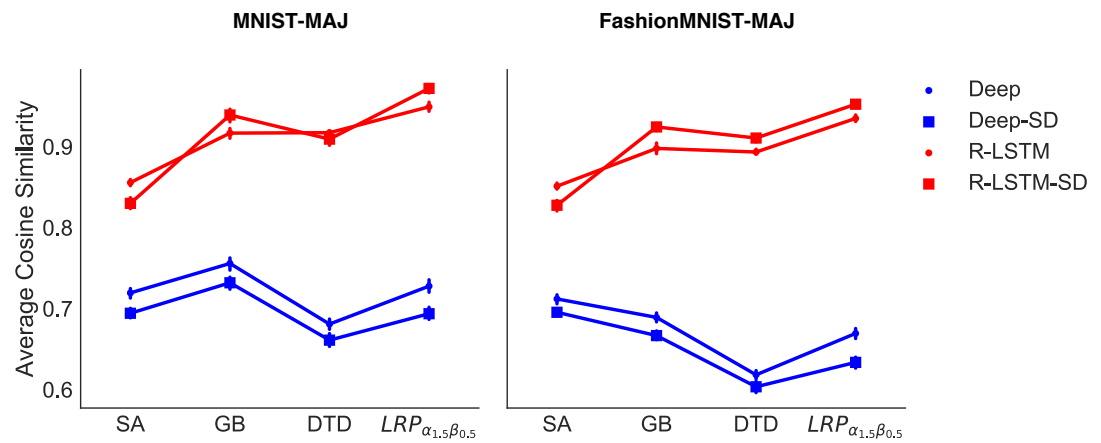


Figure 4.17: Average cosine similarity from different explanation techniques and Deep and R-LSTM architecture. The values are averaged from cross-validation results and the vertical lines depicted 95% confidence interval. The baseline is the Deep architecture depicted by dotted blue line. Accuracy of the models can be found at Appendix 1

ConvDeep with literal connections and ConvR-LSTM

For the second part, we compare the ConvDeep architecture and the effect of literal connections as well as R-LSTM-SD with convolutional layers, which is referred as ConvR-LSTM-SD. According to Figure 4.18, Conv⁺Deep produces more diffuse relevance heatmaps than ConvDeep. This is specially notable on heatmaps from SA and GB method. Similarly, Conv⁺Deep also produces worse results for DTD and LRP- $\alpha_{1.5}\beta_{0.5}$, for example consider Digit 1 and Digit 9 sample, where the relevance scores are unnecessarily distributed to the last digit's block.

Figure 4.18 also shows relevance heatmaps from ConvR-LSTM-SD whose first fully-connected layer is replaced by 2 convolutional and pooling layers. Comparing to R-LSTM-SD, having convolutional and pooling layers does improve the quality of the heatmaps further. In particular, we can clearly see samples' structures from the explanations. Figure 4.19 further emphasizes the improvement introduced by the convolutional and pooling layers. Here, we plots the relevance heatmaps by using only positive relevance. We can see that the heatmaps from ConvR-LSTM-SD are proper highlighted and provide substantial features of the samples.

Figure 4.20 presents the cosine similarity measurement this second part of the experiment. Here, ConvDeep and R-LSTM-SD are results from the previous experiments and used as baseline. Unexpectedly, having literal connections in ConvDeep does not seem to show consistent influence between MNIST-MAJ and FashionMNIST-MAJ. However, the connections considerably reduce the explanation capability of the ConvR-LSTM-SD architecture. Although explanations from ConvR-LSTM-SD are less noisy and contain impressive structures from the input as shown in Figure 4.19, the average cosine similarity of R-LSTM-SD and ConvR-LSTM-SD look almost identical. This is due to the fact our cosine similarity measurement operates on scalar values but not structures inside explanation heatmaps.

TODO : hypo: In fact, using Tukey HSD test shows that the improvement is not statistically significant
TODO : hypothesis testing



Figure 4.18: Relevance heatmaps produced by different explanation techniques on variants of ConvDeep and R-LSTM architecture trained on MNIST-MAJ and FashionMNIST-MAJ with sequence length $T = 12$. Blue indicates negative relevance, while red indicates positive relevance.

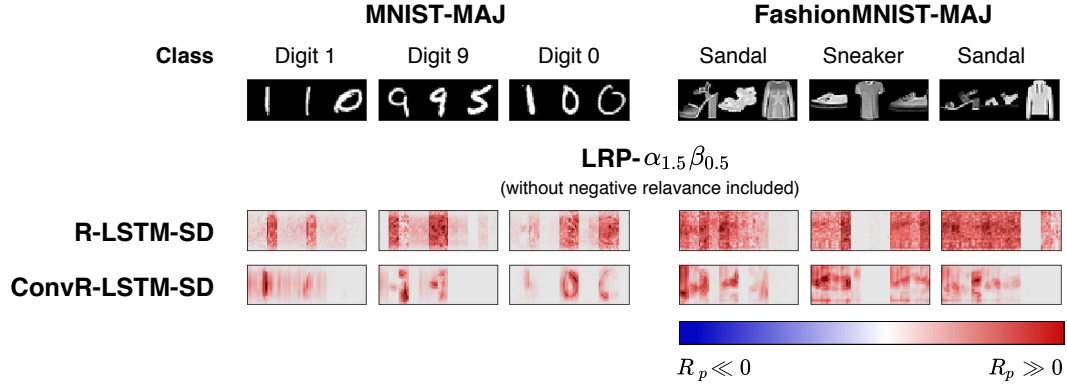


Figure 4.19: Positive relevance heatmaps produced by $LRP-\alpha_{1.5}\beta_{0.5}$ technique on R-LSTM and ConvR-LSTM architecture trained on MNIST-MAJ and FashionMNIST-MAJ with sequence length $T = 12$. Blue indicates negative relevance, while red indicates positive relevance.

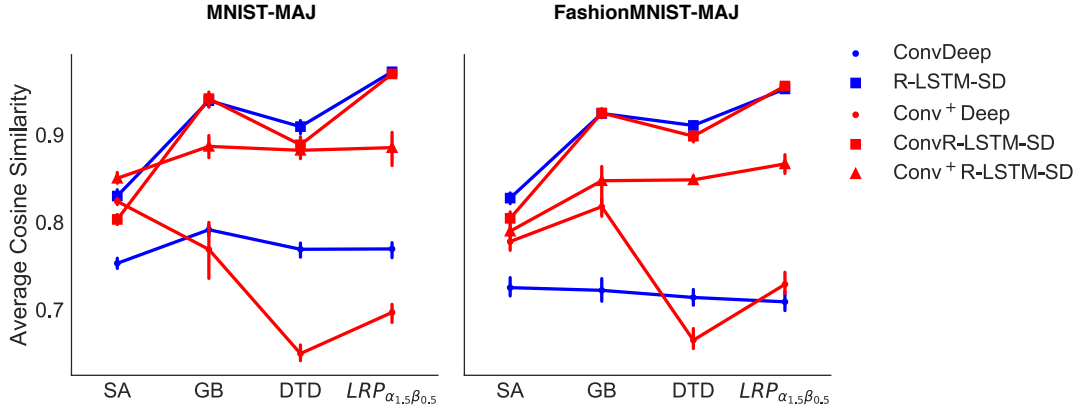


Figure 4.20: Average cosine similarity from different explanation techniques and variants of ConvDeep and R-LSTM architecture. The values are averaged from cross-validation results and the vertical lines depicted 95% confidence interval. The baseline are the Deep and R-LSTM-SD architecture represented in blue. Accuracy of the models can be found at Appendix 1

4.4.5 Summary

Results from this experiment shows some successful improvements from what we have seen on Sectoin 4.3. In particular, employing gating unit and keeping dropout activities the same significantly improve explanation ability of RNN models on any explanation method.

Moreover, convolutional and pooling layers enables the models to produce explanations with more perceivable input features than traditional fully-connected layers, although this improvement does not seem to be well captured by cosine similarity that we proposed to use. . This illustrates a shortcoming of cosine similarity that we proposed to use for the quantitative evaluation.

On the other hand, literal connections do not show any consistent improvement for the settings we are considering. In fact, having wider confidence interval suggests that they seem to make explanations less stable.

5 Conclusion

Unlike regular neural network, the quality of RNN explanation need to be considered into 2 aspects, namely local and global aspect. The local aspect describes whether explanation of each input sound. In case of image related applications, this can be improved by employing convolutional and pooling layer. On the other hand, the global aspect tells us whether RNN can properly propagate relevance quantities to the right inputs. Local explanation can not have good quality if RNN lacks capability in the global aspect.

Our experiments are artificially designed such that qualitative and quantitative evaluations can be done accordingly. The results demonstrates that the relevance propagating capability of RNN is considerably depend on the architecture of the RNN itself. In particular, deeper architecture and employing gating units significantly allows RNN to better propagate relevance scores to corresponding input.

Moreover, the level of influence from the architecture configuration is different for each explanation technique. In particular, based on our quantitative measurements, deep Taylor decomposition and Layer-Wise Relevance Propagation(LRP) are methods the most influenced by the architecture than sensitivity analysis(SA) and guided backprop(GB). Training configuration is also another factor that could affect quality of explantation. In particular, training with stationary dropout shows slight improvement on visual quality of explanation although the impact is not captured by our quantitative measurement.

Lastly, it is worth noting that we consider ConvR-LSTM-SD as the most explainable architecture in this thesis. In particular, we achieve decent explanation heatmaps when explaining it via $\text{LRP-}\alpha_{1.5}\beta_{0.5}$ without negative relevance considered. As a reminder, this result is shown on Figure 4.19.

5.1 Challenges

Throughout the time working on the thesis, we have encountered several challenges. The first challenge is about evaluations. In particular, it is quite challenging to evaluate the quality of explanations when we do not have ground truth information available. This challenge led us to artificially construct the majority sample sequence classification problem to mitigate the problem. Secondly, we have also experienced that initialization scheme of weights and biases is also another factor that could affect the quality of explanations although it would not affect the objective performance.

Lastly, because we used only basic frameworks, such as TensorFlow, and implemented most of the code ourselves, we have found that implementing neural network systems is more difficult than traditional software development in a sense that we do not have a

good way to properly verify the correctness of the code. In this aspect, we have found that properties, such as conservation property, are extremely useful because it allows us to write unit tests that automatically verify the implementation during the development. This is at least making sure that we will not make any systematic mistake in the integral part of the implementation of LRP and DTD explanation.

5.2 Future work

Despite extensive results from our experiments, we still consider our experimental setting somewhat limited. Hence, it would be better if we generalize and apply our work to broader setting. One possible future work would be applying the experiments on more diverse dataset and sequence length. Due to that fact that RNN are widely used in NLP, problems in this direction, such as text classification or sentiment analysis, are also worth experimenting.

As discussed earlier that, quantifying RNN explanation is challenging because we do not have any reliable measurement to measure local quality corresponding to each input. This leads to inconsistent results between qualitative and quantitative evaluation. Hence, another possible study could be evaluation methodology for quantifying explanation heatmaps.

References

- [Abadi et al., 2016] Abadi, M., Agarwal, A., Barham, P., Brevdo, E., Chen, Z., Citro, C., Corrado, G. S., Davis, A., Dean, J., Devin, M., Ghemawat, S., Goodfellow, I., Harp, A., Irving, G., Isard, M., Jia, Y., Jozefowicz, R., Kaiser, L., Kudlur, M., Levenberg, J., Mane, D., Monga, R., Moore, S., Murray, D., Olah, C., Schuster, M., Shlens, J., Steiner, B., Sutskever, I., Talwar, K., Tucker, P., Vanhoucke, V., Vasudevan, V., Viegas, F., Vinyals, O., Warden, P., Wattenberg, M., Wicke, M., Yu, Y., and Zheng, X. (2016). TensorFlow: Large-Scale Machine Learning on Heterogeneous Distributed Systems.
- [Arras et al., 2017] Arras, L., Montavon, G., Müller, K.-R., and Samek, W. (2017). Explaining Recurrent Neural Network Predictions in Sentiment Analysis.
- [Bach et al., 2015] Bach, S., Binder, A., Montavon, G., Klauschen, F., Müller, K.-R., and Samek, W. (2015). On Pixel-Wise Explanations for Non-Linear Classifier Decisions by Layer-Wise Relevance Propagation. *PLoS ONE*, 10(7).
- [Bach et al., 2016] Bach, S., Binder, A., Montavon, G., Muller, K.-R., and Samek, W. (2016). Analyzing classifiers: Fisher vectors and deep neural networks. In Proceedings of the IEEE Conference on Computer Vision and Pattern Recognition, pages 2912–2920.
- [Binder et al., 0906] Binder, A., Montavon, G., Lapuschkin, S., Müller, K.-R., and Samek, W. (2016/09/06). Layer-Wise Relevance Propagation for Neural Networks with Local Renormalization Layers. In Artificial Neural Networks and Machine Learning – ICANN 2016, Lecture Notes in Computer Science, pages 63–71. Springer, Cham.
- [Cho et al., 2014] Cho, K., van Merriënboer, B., Gülcühre, Ç., Bahdanau, D., Bougares, F., Schwenk, H., and Bengio, Y. (2014). Learning Phrase Representations using RNN Encoder–Decoder for Statistical Machine Translation. In Proceedings of the 2014 Conference on Empirical Methods in Natural Language Processing (EMNLP), pages 1724–1734. Association for Computational Linguistics.
- [Erhan et al., 2010] Erhan, D., Courville, A., and Bengio, Y. (October 2010). Understanding Representations Learned in Deep Architectures.
- [Gal and Ghahramani, 2016] Gal, Y. and Ghahramani, Z. (2016). A Theoretically Grounded Application of Dropout in Recurrent Neural Networks. In Lee, D. D., Sugiyama, M., Luxburg, U. V., Guyon, I., and Garnett, R., editors, Advances in Neural Information Processing Systems 29, pages 1019–1027. Curran Associates, Inc.

- [Greff et al., 2017] Greff, K., Srivastava, R. K., Koutník, J., Steunebrink, B. R., and Schmidhuber, J. (2017). LSTM: A search space odyssey. *IEEE transactions on neural networks and learning systems*.
- [He et al., 2015] He, K., Zhang, X., Ren, S., and Sun, J. (2015). Deep Residual Learning for Image Recognition. *CoRR*, abs/1512.03385.
- [Hochreiter and Schmidhuber, 1997] Hochreiter, S. and Schmidhuber, J. (1997). Long short-term memory. *Neural computation*, 9(8):1735–1780.
- [Jia et al., 2014] Jia, Y., Shelhamer, E., Donahue, J., Karayev, S., Long, J., Girshick, R., Guadarrama, S., and Darrell, T. (2014). Caffe: Convolutional Architecture for Fast Feature Embedding.
- [Jozefowicz et al., 2015] Jozefowicz, R., Zaremba, W., and Sutskever, I. (2015). An empirical exploration of recurrent network architectures. *Journal of Machine Learning Research*.
- [Kingma and Ba, 2014] Kingma, D. P. and Ba, J. (2014). Adam: A Method for Stochastic Optimization. In *Proceedings of the 3rd International Conference on Learning Representations (ICLR)*.
- [Krizhevsky et al., 2012] Krizhevsky, A., Sutskever, I., and Hinton, G. E. (2012). ImageNet Classification with Deep Convolutional Neural Networks. In Pereira, F., Burges, C. J. C., Bottou, L., and Weinberger, K. Q., editors, *Advances in Neural Information Processing Systems 25*, pages 1097–1105. Curran Associates, Inc.
- [LeCun et al., 2001] LeCun, Y., Bottou, L., Bengio, Y., and Haffner, P. (2001). Gradient-Based Learning Applied to Document Recognition. In *Intelligent Signal Processing*, pages 306–351. IEEE Press.
- [LeCun and Cortes, 2010] LeCun, Y. and Cortes, C. (2010). MNIST handwritten digit database.
- [Lee et al., 2009] Lee, H., Grosse, R., Ranganath, R., and Ng, A. Y. (2009). Convolutional Deep Belief Networks for Scalable Unsupervised Learning of Hierarchical Representations. In *Proceedings of the 26th Annual International Conference on Machine Learning, ICML '09*, pages 609–616. ACM.
- [Leon, 2017] Leon, K. (2017). Making a Simple Neural Network.
- [Melis et al., 2018] Melis, G., Dyer, C., and Blunsom, P. (2018). On the State of the Art of Evaluation in Neural Language Models. In *International Conference on Learning Representations*.
- [Montavon et al., 2017a] Montavon, G., Lapuschkin, S., Binder, A., Samek, W., and Müller, K.-R. (May 1, 2017a). Explaining nonlinear classification decisions with deep Taylor decomposition. *Pattern Recognition*, 65:211–222.

- [Montavon et al., 2017b] Montavon, G., Samek, W., and Müller, K.-R. (2017b). Methods for Interpreting and Understanding Deep Neural Networks.
- [Nguyen et al., 2016] Nguyen, A., Dosovitskiy, A., Yosinski, J., Brox, T., and Clune, J. (2016). Synthesizing the preferred inputs for neurons in neural networks via deep generator networks. In *Advances in Neural Information Processing Systems (NIPS)*.
- [Olah, 2015] Olah, C. (2015). Understanding LSTM Networks.
- [Olah et al., 2018] Olah, C., Satyanarayan, A., Johnson, I., Carter, S., Schubert, L., Ye, K., and Mordvintsev, A. (2018). The Building Blocks of Interpretability. *Distill*. <https://distill.pub/2018/building-blocks>.
- [Pascanu et al., 2012] Pascanu, R., Mikolov, T., and Bengio, Y. (2012). Understanding the exploding gradient problem. *CoRR*, abs/1211.5063.
- [Ribeiro et al., 2016] Ribeiro, M. T., Singh, S., and Guestrin, C. (2016). "Why Should I Trust You?": Explaining the Predictions of Any Classifier. In *Knowledge Discovery and Data Mining (KDD)*.
- [Simonyan et al., 2013] Simonyan, K., Vedaldi, A., and Zisserman, A. (2013). Deep Inside Convolutional Networks: Visualising Image Classification Models and Saliency Maps. *CoRR*, abs/1312.6034.
- [Simonyan and Zisserman, 2014] Simonyan, K. and Zisserman, A. (2014). Very Deep Convolutional Networks for Large-Scale Image Recognition. *CoRR*, abs/1409.1556.
- [Smilkov et al., 2017] Smilkov, D., Thorat, N., Kim, B., Viégas, F. B., and Wattenberg, M. (2017). SmoothGrad: Removing noise by adding noise. *CoRR*, abs/1706.03825.
- [Springenberg et al., 2014] Springenberg, J. T., Dosovitskiy, A., Brox, T., and Riedmiller, M. A. (2014). Striving for Simplicity: The All Convolutional Net. *CoRR*, abs/1412.6806.
- [Srivastava et al., 2014] Srivastava, N., Hinton, G., Krizhevsky, A., Sutskever, I., and Salakhutdinov, R. (2014). Dropout: A Simple Way to Prevent Neural Networks from Overfitting. *Journal of Machine Learning Research*, 15:1929–1958.
- [Sundararajan et al., 2017] Sundararajan, M., Taly, A., and Yan, Q. (2017). Axiomatic Attribution for Deep Networks.
- [Szegedy et al., 2014] Szegedy, C., Liu, W., Jia, Y., Sermanet, P., Reed, S., Anguelov, D., Erhan, D., Vanhoucke, V., and Rabinovich, A. (2014). Going Deeper with Convolutions.
- [Tieleman and Hinton, 2012] Tieleman, T. and Hinton, G. (2012). Lecture 6.5—RmsProp: Divide the gradient by a running average of its recent magnitude.

[Xiao et al., 2017] Xiao, H., Rasul, K., and Vollgraf, R. (2017). Fashion-MNIST: A Novel Image Dataset for Benchmarking Machine Learning Algorithms.

[Zagoruyko and Komodakis, 2016] Zagoruyko, S. and Komodakis, N. (2016). Wide Residual Networks.

[Zeiler, 2012] Zeiler, M. D. (2012). ADADELTA: An Adaptive Learning Rate Method. CoRR, abs/1212.5701.

[Zeiler and Fergus, 2013] Zeiler, M. D. and Fergus, R. (2013). Visualizing and Understanding Convolutional Networks. CoRR, abs/1311.2901.

Appendix

TODO : appendix : all architectures that aren't described with no. neurons

TODO : appendix : list of model accuracy and variance for hypothesis testing

Appendix 1: Accuracy on MNIST-MAJ and Fashion-MAJ models used in quantitative evaluations(Figure 4.12, 4.17, and 4.20)

dataset	architecture	count	avg_acc	std
mnist-maj	deep_v2	7	98.48	0.1274
mnist-maj	shallow	7	98.35	0.2393
mnist-maj	convrnlstm.persisted.dropout	7	99.60	0.0467
mnist-maj	deep	7	98.43	0.0926
mnist-maj	rlstm.persisted.dropout	7	98.75	0.1248
mnist-maj	rlstm	7	98.77	0.0603
mnist-maj	convtran.rlstm.persisted.dropout	7	98.30	0.1842
mnist-maj	deep.persisted.dropout	7	98.43	0.1599
mnist-maj	convdeep.transcribe	7	97.89	0.1988
mnist-maj	convdeep	7	99.28	0.0737
fashion-maj	deep_v2	7	92.07	0.3596
fashion-maj	shallow	7	92.30	0.2550
fashion-maj	convrnlstm.persisted.dropout	7	95.44	0.1356
fashion-maj	deep	7	91.35	0.3053
fashion-maj	rlstm.persisted.dropout	7	93.42	0.2513
fashion-maj	rlstm	7	93.40	0.2714
fashion-maj	convtran.rlstm.persisted.dropout	7	89.71	0.4215
fashion-maj	deep.persisted.dropout	7	91.87	0.3136
fashion-maj	convdeep.transcribe	7	89.14	0.2770
fashion-maj	convdeep	7	94.19	0.2128

Appendix 2: Hypothesis testing results of Section 4.3

```
===== Hypothesis Testing =====
for sensitivity method with significant level at 0.05
===== ANOVA =====
      sum_sq   df      F     PR(>F)
architecture  0.017522  3.0  16.995769  8.038269e-08
Residual     0.017870  52.0       NaN         NaN
effective size(eta squared) : 0.495083
```

Multiple Comparison of Means – Tukey HSD,FWER=0.05

group1	group2	meandiff	lower	upper	reject
--------	--------	----------	-------	-------	--------

convdeep	deep	-0.0353	-0.0539	-0.0167	True
convdeep	deep_v2	-0.019	-0.0376	-0.0005	True
convdeep	shallow	-0.047	-0.0656	-0.0284	True
deep	deep_v2	0.0163	-0.0023	0.0348	False
deep	shallow	-0.0117	-0.0303	0.0069	False
deep_v2	shallow	-0.028	-0.0466	-0.0094	True

```
===== Hypothesis Testing =====
for guided.backprop method with significant level at 0.05
===== ANOVA =====
      sum_sq   df      F    PR(>F)
architecture  0.021354  3.0  5.070579  0.003727
Residual     0.072995  52.0       NaN       NaN
effective size(eta squared) : 0.226326
```

Multiple Comparison of Means - Tukey HSD, FWER=0.05						
group1	group2	meandiff	lower	upper	reject	
convdeep	deep	-0.0458	-0.0834	-0.0083	True	
convdeep	deep_v2	-0.0233	-0.0609	0.0143	False	
convdeep	shallow	-0.0482	-0.0858	-0.0106	True	
deep	deep_v2	0.0226	-0.015	0.0601	False	
deep	shallow	-0.0024	-0.0399	0.0352	False	
deep_v2	shallow	-0.0249	-0.0625	0.0127	False	

```
===== Hypothesis Testing =====
for lrp_deep_taylor method with significant level at 0.05
===== ANOVA =====
      sum_sq   df      F    PR(>F)
architecture  0.469895  3.0  295.54357  1.217432e-32
Residual     0.027559  52.0       NaN       NaN
effective size(eta squared) : 0.944600
```

Multiple Comparison of Means - Tukey HSD, FWER=0.05						
group1	group2	meandiff	lower	upper	reject	
convdeep	deep	-0.062	-0.0851	-0.0389	True	
convdeep	deep_v2	-0.0169	-0.04	0.0062	False	
convdeep	shallow	-0.2313	-0.2544	-0.2082	True	
deep	deep_v2	0.0451	0.022	0.0682	True	
deep	shallow	-0.1693	-0.1924	-0.1462	True	
deep_v2	shallow	-0.2144	-0.2375	-0.1913	True	

```
=====
Hypothesis Testing =====
for lrp_alpha1_5_beta_5 method with significant level at 0.05
=====
ANOVA =====
sum_sq      df      F      PR(>F)
architecture 0.483564 3.0 260.587651 2.640318e-31
Residual     0.032165 52.0       NaN        NaN
effective size(eta squared) : 0.937632
```

Multiple Comparison of Means – Tukey HSD,FWER=0.05

group1	group2	meandiff	lower	upper	reject
convdeep	deep	-0.0344	-0.0593	-0.0094	True
convdeep	deep_v2	-0.0079	-0.0329	0.017	False
convdeep	shallow	-0.2267	-0.2516	-0.2017	True
deep	deep_v2	0.0264	0.0015	0.0514	True
deep	shallow	-0.1923	-0.2173	-0.1674	True
deep_v2	shallow	-0.2187	-0.2437	-0.1938	True
